Order Number 1336512

Correcting oil-water relative permeability data for capillary end effect in displacement experiments

Qadeer, Suhail, M.Sc.

University of Alaska Fairbanks, 1988

U·M·I
300 N. Zeeb Rd.
Ann Arbor, MI 48106

CORRECTING OIL–WATER RELATIVE PERMEABILITY DATA FOR CAPILLARY END EFFECT IN DISPLACEMENT EXPERIMENTS

By

Suhail Qadeer

RECOMMENDED:

Advisory Committee Chair

Head, Dept. of Petroleum Engineering

APPROVED:

Dean, School of Mineral Eng.

Dean of the Graduate School

Date: 9/12/88

CORRECTING OIL–WATER RELATIVE PERMEABILITY DATA FOR CAPILLARY END EFFECT IN DISPLACEMENT EXPERIMENTS

A

THESIS

Presented to the Faculty of the University of Alaska

in Partial Fulfillment of the Requirements

for the Degree of

MASTER OF SCIENCE

By

SUHAIL QADEER, B. Sc.

Fairbanks, Alaska

December, 1988

ABSTRACT

By neglecting the effect of capillary forces, the relative permeabilities calculated by the method of Johnson, Bossler, and Neumann or Jones and Roszelle from low rate displacement experiments are in error.

In this study, steady state and displacement experiments were carried out. A history matching package along with a fully implicit numerical simulator and a Welge type model were developed and the displacement data were analyzed by history matching to quantify these errors. A modified centrifuge drainage bucket was used to obtain drainage and imbibition capillary pressure data.

The results show that in the case of drainage the non–wetting phase end point relative permeabilities and saturation exponents increase with an increase in rate. However the saturation exponent for the wetting phase decreases with rate. The wetting phase end point relative permeability stayed more or less constant with rate. In the case of imbibition these parameters did not indicate any meaningful rate dependent trend.

TABLE OF CONTENTS

LIST OF TABLES

LIST OF FIGURES

ACKNOWLEDGEMENTS

I would like to express my sincere thanks to my advisor, Dr. Kaveh Dehghani, for his constant encouragement, guidance and suggestions throughout my stay at UAF. I thank Dr. David O. Ogbe for his constructive comments as a member of my committee, and for all the help he gave me for this work. I also thank Dr. Russell D. Ostermann for his help as a member of my committee, and his constructive comments during my research. Special thanks go to Dr. Ghanshyam D. Sharma for his continued support, and encouragement during my work. The financial support provided by the Petroleum Development Laboratory and the Petroleum Engineering Department is greatly appreciated. Special thanks to Dr. Lymann L. Handy of USC and Dr. Jalal Torabzadeh of California State University at Long Beach for their valuable suggestions during this study.

Last but not least my special appreciations to my wife Atiya, son Salman, and my daughter Sarah for being so patient during my studies. I dedicate this thesis to them.

1. INTRODUCTION

The single phase flow behavior in a porous medium is characterized by the absolute permeability of the media. Similarly, effective permeabilities are used to characterize the multiphase flow behavior in a porous rock. The ratio of effective to absolute permeability is called relative permeability. For petroleum engineers relative permeability is one of the most important petrophysical properties of a reservoir rock.

The methods for finding relative permeability curves can be characterized by two categories. In the first method the relative permeability curves are calculated from either the capillary pressure – saturation relationship or the grain size distribution of the rock. The second method is the direct experimental measurement of the relative permeability curves.

The experimental methods for measuring relative permeabilities can be divided into three main categories:

1 – Steady state

2 – Unsteady State

3 – History Matching

In the steady state method, the fluids are injected simultaneously into the core sample until the saturation and pressure drop across the rock sample reach a constant value. At this time the pressure drop across the core and the saturation

of the fluids in the core are measured. The pressure drop across the core along with the fluid properties used in Darcy's equation give the effective permeabilities. By varying the fluid injection rates, the relative permeability curves can be measured over the entire saturation range.

The first disadvantage of the steady state method is that it is time consuming. The second disadvantage is that the distribution of phases during the simultaneous injection of fluids through the core may not represent the actual displacement process in the reservoir (Handy and Data, 1966; Heaviside and Black, 1983).

In the unsteady state method, only one fluid, called displacing fluid, is injected into the core at either a constant rate or constant injection pressure. In the case of the constant flow rate experiments, the recovery of the displaced fluid and the pressure drop across the core is measured as a function of time. This data is analyzed by the Johnson Bossier and Neumann technique (1959) or by the graphical equivalent technique of Jones and Roszelle (1978) to calculate the relative permeabilities. In the case of constant pressure experiments the recovery and flow rates are recorded as functions of time and the data is analyzed by similar techniques.

The unsteady state method is much less time consuming than the steady state method and is more representative of the reservoir flow mechanisms. However, because the capillary forces are not considered in the analysis technique, there are inherent errors in the relative permeability curves calculated by this method. To avoid this, the experiments must be conducted at higher than reservoir flow

rates. The increased rates are known to cause fines migration (Gabrieal and Inamdar, 1983) and instability problems in adverse mobility ratio experiments (Chouke et al, 1959; Peters and Flock, 1981; Saraf and McCaffery, 1981). In 1985, Odeh and Dotson presented a method for correcting the relative permeabilities calculated by the unsteady state method for errors introduced by neglecting capillary forces. In their work they postulated that the end effect is negligible at low water saturations and high rate. They empirically found out that a plot of the ratio of oil flow rate to the oil relative permeability vs average water saturation gives a straight line in the low water saturation range. The deviation of the data points from this straight line was used to correct the experimental data. The problems associated with this technique are that most of the time the relative permeability curves are defined over a very small saturation range and the straight line may not be accurately defined.

In the history matching method the recovery and pressure drop data generated by an appropriate model is fitted to the data obtained during a displacement experiment.This method was first proposed by Archer and Wong in 1973. The relative permeability curves are adjusted until a good match is obtained with the experimental data. By history matching with a numerical simulator it is possible, to include the capillary forces. Hence, low flow rate data, which is free from problems of fines migration and instability, can be used. This method, however, does need a reliable simulator and efficient history matching package.

It is clear from the above that unsteady-state method for measuring relative permeabilities is more attractive than the steady-state method. However, errors are introduced into the relative permeability curves when the data is analyzed by the conventional JBN method or its graphical equivalent, the Jones and

Roszelle method. These errors have not yet been quantified. The objective of this study therefore was to find a functional relationship between the rate and the errors caused by neglecting capillary forces . To achieve this, error free relative permeabilities from a numerical simulator were compared with relative permeabilities calculated by a non–capillary Welge type model.

2. LITERATURE REVIEW

2.1 INTRODUCTION

The absolute permeability of a porous medium is defined as the ease with which a fluid can flow through the medium. The absolute permeability is the constant used in Darcy's law to quantify the flow of a single fluid in a porous medium saturated fully with that fluid. Darcy 's law states that the velocity of a homogeneous fluid in a porous medium is directly proportional to the pressure gradient and inversely proportional to the viscosity of the fluid, i.e.

$$v = -\frac{k}{\mu}\frac{dp}{dx} \tag{2.1}$$

The proportionality constant k, in this equation is called the absolute permeability of the porous medium, μ is the viscosity of the fluid and $\frac{dp}{dx}$ is the pressure gradient in the direction of flow.

The concept of the absolute permeability has been extended to the multi-phase flow by using the effective permeabilities for the phases occurring in the porous medium. If there are two or more fluids simultaneously present in a porous medium, each can be defined as either wetting or non-wetting phase, depending on their preferential spreading over the rock grains. The original work on the two phase flow was done by Wyckoff and Botset in 1936. They presented the idea of introducing the effective permeability into the Darcy's law to quantify two phase flow in porous media. The effective permeability to the wetting and non-wetting phases can be defined by the equations:

$$k_w = \frac{q_w \mu_w}{A(dp/dx)_w} \tag{2.2a}$$

$$k_n = \frac{q_n \mu_n}{A(dp/dx)_n} \tag{2.2b}$$

where subscripts w and n are for wetting and non-wetting phases respectively.

In 1952 Chatenever and Calhoun performed visual studies of two phase flow in glass bead models, and concluded that for a large range of flow rates during simultaneous flow, the two fluids establish their own independent tortuous paths in the porous medium forming very stable flow channels. This confirmed the applicability of Darcy's law for two phase flow.

The effective permeability to each phase increases as its saturation increases, its value is zero at the minimum saturation and increases to a maximum value at the maximum saturation of that phase. However, for comparison with other systems, the effective permeabilities are usually converted to the relative permeabilities by dividing them with a reference permeability. The choice for the reference permeability is more or less arbitrary and can be any of the following three:

a. Absolute permeability.

b. Klinkenberg corrected gas permeability.

c. Non-wetting phase effective permeability at irreducible wetting phase saturation.

It is very important to state which reference permeability has been used to convert the effective permeabilities to the relative permeabilities.

Relative permeabilities have been found to be different depending on the flow histories and direction of change in saturation, i.e. drainage or imbibition.

The drainage process is defined as the process in which the saturation of the wetting phase is decreasing. In the case of the imbibition process the saturation of the wetting phase is increasing. The difference between the imbibition and drainage relative permeability curves is known as hysteresis.

2.2 METHODS FOR DETERMINING RELATIVE PERMEABILITIES

In 1951 Geffen et al presented a comprehensive study on the different methods of determining the relative permeability curves for reservoir engineering applications. They divided the methods into the following four categories:

a. Estimation from past reservoir performance and extrapolation,

b. Use of the published laboratory data from studies on general type porous media,

c. Deriving the flow equations, using known laws of fluid dynamics, and using some experimentally measurable characteristics of the reservoir rock, and

d. Direct measurement of the flow characteristics in the laboratory on representative rock and fluid samples.

They observed that the first three methods have shortcomings which makes their use questionable. The reservoir performance data is only available for a limited type of flow process, and is not readily available during the early life of the reservoir. The data from general type porous media may not be applicable to the reservoir under consideration. The mechanism of fluid flow is not understood well enough to derive mathematical equations describing the fluid flow in the complex

pore geometry of the porous media. They concluded that the direct measurement of the relative permeability curves in the laboratory, using representative core samples from the reservoir under study, is the only reliable method of obtaining the required data. In 1981 Saraf and McCaffery published a comprehensive report on determining two and three phase relative permeabilities. They also agreed with the conclusions of Geffen at al (1951) that for the two phase flow experimentally measured relative permeabilities are better than the theoretically predicted values.

2.2.1 MATHEMATICAL MODELS FOR CALCULATING RELATIVE PERMEABILITIES

Using the basic laws of physics and fluid dynamics and some easily measurable properties of the porous medium, engineers and scientists have attempted to develop mathematical equations to describe the flow of fluids through porous media. Although there are numerous papers on this subject, none of them has been able to present equations with wide applicability because of the complicated nature of the pore structures. Work has been done to describe methods to calculate both the absolute permeability in the case of single phase flow, and to calculate the effective or relative permeabilities in the case of multiphase flow.

In 1949 Purcell used parallel capillary tubes to model the porous media and presented a model to calculate the absolute permeability from capillary pressure data. He applied Poiseuilles' equation to a bundle of capillaries of different sizes. He quantified the capillary size distribution using the capillary pressure curve to came up with the following equation:

$$k = \frac{(\sigma cos\theta)^2 F\phi}{2} \int_0^1 \frac{dS_i}{P_c} \tag{2.3}$$

In this equation F is used to correct for the differences between the flow in the hypothetical porous medium and that in natural rocks, σ is the interfacial tension between fluids, θ is the angle of contact, ϕ is the porosity and P_c is the capillary pressure. Although there were quite a few other attempts to develop equations to calculate the absolute permeability, none of them has been extended to calculate multiphase flow permeabilities . The interested reader is referred to Scheidegger (1974), Corey (1977), and Dullien (1979) for details.

As stated earlier only Purcell's work (1949) has been extended to two phase flow. Some of the important models for multi phase relative permeabilities are described in the following paragraphs.

In 1950 Gates and Lietz modified Purcell's model to develop the following equation for the relative permeability of the wetting phase,

$$k_{rw} = \frac{\int_0^{S_w} \frac{dS_w}{P_c^2}}{\int_0^1 \frac{dS_w}{P_c^2}} \tag{2.4}$$

In 1951 Narr and Dykstra postulated that the tortuosity factor τ,which is a measure of the deviation of the flow path in porous media from straight capillaris, should be a function of saturation, and therefore it should be included in the integral in equation 2.4. They assumed τ to be inversely proportional to the radius of the capillary and obtained the following equation:

$$k_{rw} = \frac{\int_0^{S_w} \frac{dS_w}{P_c^3}}{\int_0^1 \frac{dS_w}{P_c^3}} \tag{2.5}$$

Applying this equation to the data from Gates and Lietz and their own data they concluded that the relative permeability curves predicted by their equation matches the experimental data better than the Gates and Lietz's data.

In 1953 Burdine extended his earlier work (Burdine et al, 1950) on absolute permeability, and observed that the tortuosity factor depends on the saturation of the wetting phase. He presented the following equation to approximate the tortuosity factor:

$$\tau = \left(\frac{S_w - S_{wi}}{1 - S_{wi}}\right)^2 \tag{2.6}$$

The wetting phase relative permeability is then given by:

$$k_{rw} = \left(\frac{S_w - S_{wi}}{1 - S_{wi}}\right)^2 \frac{\int_0^{S_w} \frac{dS_w}{P_c^2}}{\int_0^1 \frac{dS_w}{P_c^2}} \tag{2.7}$$

This equation fitted their experimental data quite well. Defining a similar tortuosity factor for the non-wetting phase as:

$$\tau_n = \left(1 - \frac{S_w - S_{wi}}{S_m - S_{wi}}\right)^2 \tag{2.8}$$

where S_m is the lowest wetting phase saturation for which the non-wetting phase tortuosity factor is infinite (Corey, 1954), the non-wetting phase relative permeability can be defined by the equation:

$$k_{rn} = \left(1 - \frac{S_w - S_{wi}}{S_m - S_{wi}}\right)^2 \frac{\int_0^{S_w} \frac{dS_w}{P_c^2}}{\int_0^1 \frac{dS_w}{P_c^2}} \tag{2.9}$$

This equation did not fit the experimental data for non-wetting phase relative permeability as well as that given by equation 2.7 for the wetting phase.

In 1954 Corey found that for gas–oil system, the expression:

$$\frac{1}{P_c^2} = \begin{cases} \frac{c(S_o - S_{or})}{1 - S_{or}} & \text{for } S_o > S_{or} \\ 0 & \text{for } S_o < S_{or} \end{cases} \tag{2.10}$$

was a good approximation. Where c in this equation is the geometric constant in Kozeny equation. Substituting this equation in equation 2.9 and integrating gives the following equations for the drainage case :

$$\begin{aligned} k_{rn} &= \left(1 - \frac{S_o - S_{or}}{1 - Sor}\right)^2 \left[1 - \left(\frac{S_o - S_{or}}{1 - S_{or}}\right)^2\right] \\ &= (1 - S_{oe})^2(1 - S_{oe}^2) \end{aligned} \tag{2.11a}$$

and,

$$\begin{aligned} k_{rw} &= \left(\frac{S_o - S_{or}}{1 - S_{or}}\right)^4 \\ &= S_{oe}^4 \end{aligned} \tag{2.11b}$$

where S_{oe} is the effective oil saturation given by:

$$S_{oe} = \frac{S_o - S_{or}}{1 - S_{or}} \tag{2.11c}$$

and S_m has been taken equal to one. The above expressions can be used to calculate relative permeabilities to both oil and gas.

It is well known that the saturation history is an important parameter in multi phase flow in porous media. The above equations hold very well in case of drainage, but in the case of imbibition the calculated relative permeabilities are higher than experimentally determined values.

In 1961 Narr and Henderson developed a mathematical model for consolidated porous media. They modified the Wyllie–Gardner theory (1958a and 1958b)

by assuming that one half of the initial non-wetting phase saturation will finally be trapped by the advancing wetting phase. They defined a flowing non-wetting phase saturation; $S_{nf} = S_n - S_{nt}$ and a reduced saturation S^*_{nf}, given by:

$$S^*_{nf} = \frac{S_o - S_{nt}}{1 - S_{wi}} \tag{2.12}$$

where S_{nt} is the trapped non-wetting phase saturation. If it is assumed that:

$$\frac{1}{P_c^2} = cS^*$$

and the non-wetting phase reduced flowing saturation S^*_{nf} is defined by:

$$S^*_{nf} = \frac{S_n - S_{nt}}{1 - S_{wi}} \tag{2.13}$$

then the non-wetting phase imbibition relative permeability is given by:

$$k_{rn(imb)} = {S^*_{nf}}^3 \left[S^*_{nf} + 3(S^*_{wf} + S^*_{nt})\right] \tag{2.14}$$

where,

$$S^*_{wf} = \frac{S_w - S_{wi}}{1 - S_{wi}} \tag{2.15}$$

and

$$S^*_{nt} = \frac{S_{nt}}{1 - Swi} \tag{2.16}$$

The relative permeability to the wetting phase is given by:

$$k_{rw(imb)} = {S^*_{wf}}^4 \tag{2.17}$$

Although Narr and Henderson (1961) have provided a model which accounts for trapping of the non-wetting phase in an imbibition process, the quantification of the trapped phase is rather arbitrary. Narr, Wygal and Henderson (1962) observed that for unconsolidated sands, the imbibition non-wetting phase

relative permeability is higher than that for drainage. This observation is opposite to that observed for consolidated sands, and the model would fail in case of unconsolidated sands. This can possibly be attributed to the differences in pore size distribution and cementation.

In 1980 Morrow and Chatiudompunth calculated the hydraulic radius of each phase from drainage and imbibition capillary pressure and surface area measurements on packs of spheres. They found that the hydraulic radius of the non–wetting phase has hysteresis similar to that shown by non–wetting phase relative permeabilities in unconsolidated sands.

In 1969 Ashford modified the Narr–Henderson theory by introducing a correction factor, which depends on the particular matrix. He observed that the trapping predicted by their theory gives an upper limit which is higher than the actual case.

It has been pointed out by Saraf and McCaffery (1981) that none of these models has been widely tested. It is therefore advisable to use experimental methods of relative permeability measurement. A brief description of the experimental methods of determining relative permeability curves follows in the next section.

2.2.2 EXPERIMENTAL METHODS FOR MEASURING RELATIVE PERMEABILITIES

The experimental methods of measuring relative permeabilities can be divided into two main classes, i.e. steady state and displacement or unsteady state.

2.2.2.1 STEADY STATE METHODS

In the steady state method, both wetting and non-wetting phases are injected simultaneously into the core. The pressure drop across the core along with the viscosities of the fluids are used in the Darcy's law to calculate the relative permeabilities. The saturation of the wetting phase can be varied by changing the ratio of flow rates of the fluids, and hence the relative permeability curves can be defined over the entire saturation range. It was pointed out by earlier researchers (Terwilliger et al.,1951; Richardson, 1957; Johnson et al., 1959) that both steady state and unsteady state methods give comparable results. Later works by Handy and Data (1966) and Amaefule and Handy (1981) have indicated that the saturation distribution and hence the relative permeabilities are different for steady state and displacement process. The saturation determination and distortion in saturation distribution at the outlet end are the two main problems associated with the steady state methods(Caudle et al.,1951; and Geffen et al., 1951). The following are the four main classifications of steady state methods:

A. Static (Stationary Fluid) Methods:

In this method an attempt is made to keep one of the fluid stationery by placing semi-permeable plates at both ends of the core. In 1951 Osoba et al. used semi-permeable plates which allowed only gas to flow. They were thus able to measure the relative permeability to gas in the presence of a liquid phase. In 1951 Rapoport and Leas allowed the liquid to flow keeping the gas phase stationary. They measured the liquid permeability by this method. In 1962 Loomis and Crowell used a combination of these two to measure the relative permeabilities to

both phases. In this method since one of the mobile phases is not allowed to flow, the flow mechanism is unrealistic and the results obtained are questionable.

B. Hassler Capillary Method

In 1944 Hassler presented a method in which semi–permeable membranes are provided at both ends allowing the fluids to flow separately outside the core. The fluids are allowed to commingle and flow simultaneously inside the core. Pressures are measured in each phase through the semi–permeable plates and the pressure difference between the phases is kept constant throughout the core to eliminate the capillary end effect. Saturations are altered by altering the capillary pressure in the system. In 1951 Osoba et al. reported that this method gives relative permeabilities which are consistently lower than the dynamic or Penn–State method. This method is very slow, and hence it is not used commonly.

C. Penn–State or Dynamic Method

In 1947 Morse et al. while working at Pennsylvania State University developed this method, in which both fluids are allowed to flow simultaneously through the core without the use of any barriers at the inlet or the outlet end. In this method three pieces of the same porous medium are used in a core holder. The upstream piece acts as a mixing zone, where incoming wetting and non–wetting phases mix together. Pressure drop and saturations are measured in the middle section. The end effect is confined to the down stream section. In 1951 Caudle et al., Osoba et al., and Geffen et al. used this method and reported reliable and consistent results. The capillary contact between different sections of the core and the saturation determination pose a problem in this method. The core needs to

be taken out of the core holder and weighed after each saturation change. This causes erroneous results because of loss of fluid during this process. This may occur either because of evaporation loss or gas expansion during measurements of gas–liquid systems. In 1951 Osoba et al. used a single core instead of three to avoid the problem of capillary contact between the three pieces They showed that end effects could be minimized by using higher flow rates. Another possibility is that saturation may be determined in–situ away from the inlet and outlet ends. Under these conditions the modified Penn–state method is by far the best technique available for measuring the relative permeabilities by steady state method.

D. Quasi Steady State Methods

In 1936 Hassler et al. injected only gas in small bursts at the inlet end, which caused the liquid to flow. This in reality is a gas drive method in steps over short periods of time and hence can be considered a quasi steady state method.

The other method in this classification is the gas drive. In this method the liquid is displaced by the gas coming out of solution in the core as a result of lowering the pressure of the liquid containing gas at its bubble point. This method was proposed by Brownscombe et al. in 1950. The mechanism of flow is different from either dynamic or steady state but is appropriate for reservoirs producing under solution gas drive.

As pointed out the two main problems associated with the steady–state methods are the capillary end effect and saturation measurement. The capillary end effect can be confined either to a very small section near the outlet end, or to the out let end piece as proposed by Hassler (1944). In either case, the

determination of the true saturation is important. Saturations may be determined by any one of the following techniques:

(a) Gravimetric Balance,

(b) Volumetric Balance,

(c) Resistivity Measurements, and

(d) Radiation Absorption,

(a) Gravimetric Balance

In this method the core assembly needs to be dismantled at the end of each saturation change. The core is weighed before the start of the experiment and then after each saturation change. By knowing the density difference of the two fluids in the core and change in weight, the saturations can be calculated from the weight balance. This method has the disadvantage that there is fluid loss from the core because of fluid expansion and evaporation.

(b) Volumetric Balance

In this method an account of the volumes of the fluids injected and produced from the core at any saturation step is maintained . The volume of the fluids in the tubing must be considered if the dead volume of the tubing is not negligible to the pore volume of the core. The core does not need to be dismantled in this method but it provides only an average value for the entire core and hence the end effect must be confined to a small section of the core.

The use of this technique is further facilitated by the method of recirculation of fluids proposed by Hvolboll (1978) and used by Braun and Blackwell

(1981), Torabzadeh and Handy (1984) and Saraf et al (1982). In this method fluids are produced into a separator and reinjected into the core. The change in the oil–water interface in the separator gives the volumetric balance of the fluids in the core. This change is measured visually (Torabzadeh and Handy, 1984) , or by computer based photometric scanning (Saraf et al, 1982). Other measuring techniques which could be used include monitoring hydrostatic pressures associated with head change (Torabzadeh and Handy, 1984) or by ultrasonic reflectometry.

(c) Resistivity Measurement

One of the fluids must be conductive to electricity for this method. A very small alternating current is passed through the core. Potential measuring electrodes are placed along the length of the core. The resistivity is measured by balancing a resistance bridge, one leg of which is the section of the core. A calibration curve is drawn by measuring the resistance of small core samples having a known saturation. This calibration curve is used to determine the saturation from the resistivity measurements. Although the current is kept small, local polarization causes the readings to be erratic.

(d) Radiation Absorption

Several radiation absorption techniques have been used by different investigators. These are: microwave, x–rays, and gamma rays for this purpose. A calibration curve is constructed using data obtained from small core samples, with known saturation. Because of the distortion this method does not work well near the end of the core.

2.2.2.2 UNSTEADY STATE METHODS

In case of displacement or unsteady-state method of measuring relative permeability only one of the fluids is injected into the core. The core is at irreducible saturation of the displacing fluid. The pressure drop and recovery data are recorded during the experiment. The methods used to calculate relative permeabilities from this data can be divided into two groups. The first one is the conventional Johnson, Bossler, and Neumann (1959) and its modification by Jones and Roszelle (1978). These methods are based on the Welge's displacement model (1952). Welge's model is based on fractional flow equation presented by Leverett in 1941, which can be written as:

$$f_w = \frac{1 + \frac{k_o}{q_t \mu_o}\left[\frac{\partial P_c}{\partial x} - g\triangle\rho \sin\theta\right]}{1 + \frac{k_o \mu_w}{k_w \mu_o}} \tag{2.18}$$

Welge after neglecting the capillary and gravity forces obtained

$$\overline{S_w} - S_{w2} = f_{o2} Q_w \tag{2.19}$$

where $\overline{S_w}$ is the average water saturation and f_{o2} is the fractional flow of oil at the outlet end of the core. The subscript 2 refers to the values measured at the outlet end of the core. Q_w is the cumulative water injected into the core in pore volume. A plot of Q_w vs $\overline{S_w}$ is used to find f_{o2} and S_{w2} as slope and intercept. f_{o2} is related to the ratio of permeabilities, k_{rw} and k_{ro} by:

$$f_{o2} = \frac{1}{1 + \frac{k_{rw}\mu_o}{k_{ro}\mu_w}} \tag{2.20}$$

A similar expression can be obtained from the Buckley-Leverett (1942) theory of frontal advance.Both of these derivations assume capillary and gravity forces to

be negligible when compared to the viscous forces. The capillary forces can be neglected if the second term in the numerator of equation (2.16) can be neglected. In practice this is achieved by increasing the flow rate q_t. In 1953 Rapoport and Leas found that waterflooding can be scaled linearly, i.e. the fluid saturations at any time and position is a function of the number of pore volumes injected only. Based on this concept they defined a scaling parameter $lv\mu_w$, and experimentally found a critical value for this parameter above which the flow is stabilized. When designing flow experiments, for measuring relative permeabilities by this method, it is therefore important to keep the scaling parameter high enough to ensure stabilized flow.

In 1959 Johnson et al., extending the work of Welge, presented the following equations which allowed them to calculate individual relative permeabilities from displacement experiments. The method is known as JBN method.

$$k_{ro} = \frac{f_{o2}}{d\left(\frac{1}{Q_w I_r}\right)/d\left(\frac{1}{Q_w}\right)} \tag{2.21}$$

and,

$$k_{rw} = \frac{f_{w2}}{f_{o2}} \frac{\mu_w}{\mu_o} k_{ro} \tag{2.22}$$

These equations give the relative permeabilities at the outlet face of the core which is related to the outlet face saturation through equation (2.19). The term I_r defined as relative injectivity is given by:

$$I_r = \frac{Q_w/\triangle P}{(Q_w/\triangle p)_{init}} \tag{2.23}$$

In 1978 Jones and Roszelle developed a method that is graphical equivalent to the JBN method. They claimed that their technique is easier to use than JBN

and is less prone to errors caused by differentiation of data as required in the JBN method. In 1973 Archer and Wong reported that the JBN and its other equivalent methods give erroneous relative permeabilities when used for strongly water wet cores where the displacement process is piston like, or the cores are heterogeneous.

Archer and Wong(1973) were the first to propose history matching of the laboratory core flood data by a trial–and–error procedure to obtain relative permeabilities. This concept of history matching has been further extended by Sigmund and McCaffery (1979) when they proposed the use of a semi–automatic history matching routine based on the Newton–Raphson technique.

In 1986 Watson et al. used a Levenberg–Marquardt algorithm to history match laboratory data and to calculate the relative permeabilities. Their method provides a better convergence compared to the earlier methods. They also proposed the use of cubic splines to represent the relative permeability curves. They claimed that cubic splines represent the true relative permeability curves more accurately. However the extra work required to obtain the cubic spline parameters, and little improvement over conventional exponential representation of relative permeability curves does not justify the use of cubic splines.

It can be realized from this discussion that the displacement experiments conducted at low rates better represent the reservoir flow mechanism. Because of neglecting the capillary forces, present techniques of calculating relative permeabilities by either the JBN or the Jones and Roszelle methods give erroneous results. These errors have not yet been quantified. In this study an attempt is made to quantify these errors by finding a functional relationship between flow rate and the errors. A history matching algorithm is used with two models, a

numerical simulator which takes into account the capillary end effect, and a non-capillary Welge type model to find this relationship. These models are described in the next chapter.

3. SOFTWARE DEVELOPMENT

The first task in this study is to develop the necessary software. This included developing three computer programs. The first of these was a finite difference, fully implicit, numerical simulator, including capillary end effect. The second is a non–capillary Welge type model. The third one is an automatic history matching package that uses the Levenberg–Marquardt algorithm. The mathematical formulation of these programs is discussed in the following sections.

3.1 THE NUMERICAL SIMULATOR

The finite difference simulator, developed in this study is a one dimensional, incompressible, two–phase simulator for horizontal cores. The development closely follows the approach presented by Aziz and Settari (1979). The general equation for two phase flow in one dimension can be written as:

$$\frac{\partial}{\partial x}\left(\lambda_l \frac{\partial p_l}{\partial x}\right) = \frac{\partial}{\partial t}\left(\phi \frac{S_l}{B_l}\right) + q_l \tag{3.1}$$

where,

$$l = w, n = \text{wetting and non–wetting phase}$$

capillary pressure p_c is:

$$p_c = p_n - p_w \tag{3.2}$$

sum of saturations is:

$$S_w + S_n = 1 \tag{3.3}$$

and the transmissibility is defined as:

$$\lambda_l = \frac{k_{rl}}{\mu_l B_l} k \tag{3.4}$$

Considering an incompressible system with constant μ_l and setting $\beta_c = 1$, equation (3.1) can be written as:

$$\frac{k}{\mu_l}\frac{\partial}{\partial x}\left(k_{rl}\frac{\partial p_l}{\partial x}\right) = \phi\frac{\partial S_l}{\partial t} + q_l \tag{3.5}$$

The next step in the formulation of the problem is the specification of the boundary conditions. In the linear flow system, the inlet and the outlet end of the core form the boundaries where the flow conditions need to be specified. In this model the inlet boundary condition is specified by setting a constant rate of injection of fluids into the system. The outlet boundary condition needs to be more elaborate because of the outlet capillary end effect. This outlet end effect is the result of a capillary discontinuity between the outlet face of the core and the fluid filled space just outside the core. There is no flow of the wetting phase out of the core until the capillary pressure at the outlet face of the core becomes equal to that outside the core, which is usually taken as zero. This occurs when the saturation of the wetting phase has increased to S_{w0}, the saturation corresponding to zero capillary pressure. After this stage the flow of the wetting phase out of the core is controlled by the Darcy's law (Settari and Aziz, 1974). Mathematically, this can be written as;

$$q_w = \begin{cases} 0 & \text{if } S_w < S_{w0} \\ \lambda_w \frac{\partial p_w}{\partial x} & \text{if } S_w = S_{w0} \end{cases} \tag{3.6}$$

Equation (3.5) along with the boundary conditions given by equation (3.6) are solved by the simultaneous solution method patterned after Aziz and Settari (1979). In this study I have used the point distributed grid. The saturation term in the right side of equation 3.5 is discretized by a backward difference approximation as:

$$\frac{\partial S_l}{\partial t} \simeq \frac{1}{\Delta t}\Delta_t(S_l) \tag{3.7a}$$

where,

$$\Delta_t(S_l) = S_l^{n+1} - S_l^n \tag{3.7b}$$

If we define;

$$T_{i+1/2} = \frac{\lambda_{i+1/2} A}{\Delta x_{i+1/2}} \tag{3.8a}$$

and,

$$V_{pi} = \phi_i A_i \Delta x_i \tag{3.8b}$$

equation 3.5 can be discretized as;

$$\left[\Delta T_l \Delta p_l^{n+1}\right]_i = \frac{V_{pi}}{\Delta t} \Delta_t (S_l) + Q_{li} \tag{3.9}$$

where,

$$\Delta T \Delta p \equiv T_{i+1/2}[p_{i+1} - p_i] + T_{i-1/2}[p_{i-1} - p_i] \tag{3.10}$$

and Q_{li} is the block injection rate.

The next important step in the formulation of the simultaneous solution method is writing the right hand side in terms of p_w and p_n. To accomplish this, we can write:

$$\Delta_t(S_l) = \frac{S_l^{n+1} - S_l^n}{P_c^{n+1} - P_c^n} \Delta_t P_c \tag{3.11}$$

With these definitions we can write the final equation in finite difference form at each grid block as:

$$\begin{aligned} [\Delta T_w \Delta \mathbf{p}_w]_i^{n+1} &= [d_{11} \Delta_t p_w + d_{12} \Delta_t p_n]_i + Q_{wi} \\ [\Delta T_n \Delta p_n]_i^{n+1} &= [d_{21} \Delta_t p_w + d_{22} \Delta_t p_n]_i + Q_{ni} \end{aligned} \tag{3.12}$$

where the coefficients d_{kl} are defined as:

$$d_{11} = d_{22} = -\frac{V_p}{\Delta t} S_w' \tag{3.13}$$

$$d_{12} = d_{21} = \frac{V_p}{\Delta t} S'_w \tag{3.14}$$

There are two equations for each grid block which are solved simultaneously. These equations can be written in matrix form as:

$$\mathbf{T}\vec{\mathbf{P}}^{n+1} = \mathbf{D}(\vec{\mathbf{P}}^{n+1} - \vec{\mathbf{P}}^{n}) + \vec{\mathbf{Q}} \tag{3.15}$$

where $\mathbf{T}$ is an $N \times N$ transmissibility matrix, $\mathbf{D}$ is an $N \times N$ diagonal matrix, $\vec{\mathbf{Q}}$ is $1 \times N$ source vector, and $\vec{\mathbf{P}}$ is an $1 \times N$ vector of pressures are each grid point. In the subsequent discussion bold face letters denote either a matrix or a vector, whereas elements of the matrices and vectors are denoted by italics.

Each 'block row' in these matrices corresponds to a block. The ith block row of matrix $\mathbf{T}$ is:

$$\begin{bmatrix} T_{wi-1/2} & 0 & -(T_{wi-1/2}+T_{wi+1/2}) & 0 & T_{wi+1/2} & 0 \\ 0 & T_{ni-1/2} & 0 & -(T_{ni-1/2}+T_{ni+1/2}) & 0 & T_{ni+1/2} \end{bmatrix} \tag{3.16}$$

The corresponding block element of $\mathbf{D}$ is a 2×2 matrix;

$$\mathbf{D}_i = \begin{bmatrix} d_{11i} & d_{12i} \\ d_{21i} & d_{22i} \end{bmatrix} \tag{3.17}$$

$\vec{\mathbf{P}}$ is the vector of pressures in both phases at each block;

$$\vec{\mathbf{P}} = [p_{w1}, p_{n1}, \ldots, p_{wN}, p_{nN}]^T \tag{3.18}$$

Equation (3.15) can be written in residual form which is more convenient from the computational point of view. Defining an R^k for any P^k as:

$$\vec{\mathbf{R}}^k = \mathbf{T}\vec{\mathbf{P}}^k - \mathbf{D}(\vec{\mathbf{P}}^k - \vec{\mathbf{P}}^n) \tag{3.19}$$

Then the solution of equation (3.15) satisfies

$$\vec{\mathbf{R}}^{n+1} = \vec{\mathbf{Q}} \tag{3.20}$$

We can write equation 3.15 for each time step as:

$$(\mathbf{T}-\mathbf{D})(\vec{\mathbf{P}}^{n+1}-\vec{\mathbf{P}}^{n})=-\vec{\mathbf{R}}^{n}+\vec{\mathbf{Q}} \tag{3.21}$$

In the iterative procedure we need some approximation $\vec{\mathbf{P}}^{k}$ for $\vec{\mathbf{P}}^{n+1}$, so that the last iteration can be written as:

$$(\mathbf{T}-\mathbf{D})(\vec{\mathbf{P}}^{n+1}-\vec{\mathbf{P}}^{k})=-\vec{\mathbf{R}}^{k}+\vec{\mathbf{Q}} \tag{3.22}$$

This equation is solved by the fully implicit method. This requires an iterative procedure for solving the system of equations. The next paragraphs describe the method used for solving the system of equations.

The shapes of the relative permeability and the capillary pressure curves cause strong non-linearities in the $\mathbf{T}$ and $\mathbf{D}$ matrices. The non-linearity in the $\mathbf{T}$ matrix has two aspects. One is the approximation of $\mathbf{T}_{i+1/2}$ in the space coordinate, which is called transmissibility weighting problem. In this study I have used a single point upstream weighting of the transmisibilities. As the flow in this model is always from block i to $i+1$, we can write

$$k_{rl_{i+1/2}}=k_{rl_{i}} \tag{3.23}$$

to accomplish this weighting procedure.

The other approximation needed for the fully implicit solution of the equations is in the representation of the $\mathbf{T}$ and $\mathbf{D}$ matrices at the $n+1$ time level. In this simulator we have used Newtons method for the nonlinearity in the $\mathbf{T}$ matrix. These iterations are called the main iterations. Sub iterations for each main iteration are performed on the $\mathbf{D}$ matrix, using a modified Newtons method (Settari and Aziz, 1978).

The Newtons method for the solution of equation 3.15 can be written as:

$$\mathbf{DR}^{v}[\vec{\mathbf{P}}^{v+1} - \vec{\mathbf{P}}^{v}] = -\vec{\mathbf{R}}^{v} + \vec{\mathbf{Q}} \tag{3.24a}$$

Note:

$$v = 0, 1, \ldots; \vec{\mathbf{P}}^{0} = vp^{n} \tag{3.24b}$$

and $\mathbf{DR}$ is the Jacobi matrix of $\vec{\mathbf{R}}$. For the main iteration we assume that $\mathbf{D}$ is constant. The block element of $\mathbf{DR}$ in the ith row and jth column will be:

$$\begin{bmatrix} \frac{\partial R_{wi}}{\partial p_{wj}} & \frac{\partial R_{wi}}{\partial p_{nj}} \\ \frac{\partial R_{ni}}{\partial p_{wj}} & \frac{\partial R_{nj}}{\partial p_{nj}} \end{bmatrix} \tag{3.25}$$

where $l, k = w, n$. The matrix $\mathbf{DR}$ will have only non-zero elements in the locations of three block diagonal elements of the matrix $\mathbf{T}$.

The ith-element of vector $\mathbf{T}\vec{\mathbf{P}}$ may be written as:

$$\mathbf{T}\vec{\mathbf{P}} = -T_{l_{i-1/2}}(p_{l_i} - p_{l_{i-1}}) + T_{l_{i+1/2}}(p_{l_{i+1}} - p_{l_i}) \tag{3.26a}$$

or in a concise form:

$$\mathbf{T}\vec{\mathbf{P}} = -(T\Delta p)_{l_{i-1/2}} + (T\Delta p)_{l_{i+1/2}}$$

$$l = w, n \tag{3.26b}$$

The three non-zero elements of the ith row of matrix $\mathbf{DR}$ are found by differentiating equation 3.26a with respect to p_{i-1}, p_i, and p_{i+1}. These three elements are:

$$\frac{\partial}{\partial p_{k_{i+1}}}[(T\Delta p)_{l_{i+1/2}} - (T\Delta p)_{l_{i-1/2}}] = \delta_{kl} T_{l_{i+1/2}} \tag{3.27}$$

$$\frac{\partial}{\partial p_{k_i}}[(T\Delta p)_{l_{i+1/2}} - (T\Delta p)_{l_{i-1/2}}] = -\delta_{kl} T_{l_{i+1/2}} + T'_{l_{i+1/2}} \frac{\partial P_{c_i}}{\partial p_{ki}} - \delta_{kl} T_{l_{i-1/2}} \tag{3.28}$$

$$\frac{\partial}{\partial p_{k_{i-1}}}[(T\Delta p)_{l_{i+1/2}} - (T\Delta p)_{l_{i-1/2}}] = \delta_{kl} T_{l_{i-1/2}} - T'_{l_{i-1/2}} \frac{\partial P_{c_{i-1}}}{\partial p_{k_{i-1}}} \tag{3.29}$$

where:

$$\delta_{kl} = \begin{cases} 1, & \text{if } k = l \\ 0, & \text{if } k \neq l \end{cases} \tag{3.30}$$

$$k = n, w$$

and,

$$T'_{l_{i+1/2}} = \Delta p_{l_{i+1/2}} \frac{\partial T_{l_{i+1/2}}}{\partial P_{c_i}} \tag{3.31}$$

Since the derivative of $\mathbf{D}\vec{\mathbf{P}}$ is $\mathbf{D}$, after collecting all terms the matrix $\mathbf{DR}$ can be written as:

$$\mathbf{DR} = \mathbf{T} + \mathbf{T}' - \mathbf{D} \tag{3.32}$$

In equation (3.32), $\mathbf{T}'$ is a matrix composed of $\mathbf{T}'_l$. Substituting equation (3.32) into (3.24a) gives:

$$(\mathbf{T}^v + \mathbf{T}'^v - \mathbf{D})(\vec{\mathbf{P}}^{v+1} - \vec{\mathbf{P}}^v) = -\vec{\mathbf{R}}^v + \vec{\mathbf{Q}}$$

note:

$$v = 0, 1, \ldots; P^0 = P^n \tag{3.33}$$

In the sub–iterations to update matrix $\mathbf{D}$, it is assumed that matrix $\mathbf{T}$ is constant and a modified Newtons method is applied to equation (3.33). A vector $\vec{\mathbf{DS}}$ is defined as:

$$\vec{\mathbf{DS}}^{n,n+1} = \mathbf{D}^{n+1}(\vec{\mathbf{P}}^{n+1} - \vec{\mathbf{P}}^n) \tag{3.34}$$

The derivative of $\vec{\mathbf{DS}}$ is $\mathbf{D}$. Substituting this term into equation 3.33 and applying Newtons method, we get:

$$(\mathbf{T}^n + \mathbf{T}'^n - \mathbf{D}^v)(\vec{\mathbf{P}}^{v+1} - \vec{\mathbf{P}}^v) = -\vec{\mathbf{R}}_n^n - (\mathbf{T}^n + \mathbf{T}'^n)(\vec{\mathbf{P}}^v - \vec{\mathbf{P}}^n) + \vec{\mathbf{DS}}^{n,v} + \vec{\mathbf{Q}} \tag{3.35}$$

Note:

$$v = 0, 1, \ldots, P^0 = P^n \tag{3.36}$$

Let $\vec{\mathbf{P}}^*$ be the solution of the equation (3.35) in the $(v+1)$th iteration. As the inverse function p_c, the capillary pressure is explicitly known, we can calculate the saturation vector $\vec{\mathbf{S}}^{v+1}$ using:

$$S_{w_i}^{v+1} = \left[\frac{dS_w}{dP_c}\right]_i^v [p_c^* - p_c^v]_i + S_{wi}^v \tag{3.37}$$

For all grid points, the pressure vector $\vec{\mathbf{P}}^{v+1}$ is calculated by:

$$\vec{\mathbf{P}}_n^{v+1} = \vec{\mathbf{P}}_n^* \tag{3.38}$$

$$\vec{\mathbf{P}}_w^{v+1} = \vec{\mathbf{P}}_o^{v+1} - \vec{\mathbf{P}}_c(S_w^{v+1}) \tag{3.39}$$

This modified Newtons method has a very good rate of convergence (Settari, 1973).

As already discussed, the iterative scheme has two levels of iterations. The inner level represents iterations on matrix $\mathbf{D}$ according to equation (3.35); they are denoted by superscript v. The outer level represents Newton's iterations on matrix $\mathbf{T}$ (equation 3.33), and are represented by superscript k. We define two more vectors $\vec{\mathbf{RS}}$ the residual vector and $\Delta\vec{\mathbf{RS}}$ the incremental residual vector over one inner-iteration as:

$$\vec{\mathbf{RS}}^v = \mathbf{T}\vec{\mathbf{P}}^v - \mathbf{D}\vec{\mathbf{S}}^{n,v} \tag{3.40}$$

$$\Delta\vec{\mathbf{RS}}_k^v = [\mathbf{T} + \mathbf{T}']^k[\vec{\mathbf{P}}^{k+1,v} - \vec{\mathbf{P}}^{k+1,(v-1)}] + \mathbf{D}\vec{\mathbf{S}}^{(v-1),v} \tag{3.41}$$

Using these definitions, the overall iteration scheme can be written as:

$$\left[(T+T')^{k-1} - D^{k,v}\right](P^{k,(v+1)} - P^{k,v}) = -\left[RS_{k-1}^{k-1} + \sum_{\epsilon=0}^{v} \Delta RS_{k-1}^{\epsilon}\right] + Q^{k,v}$$

$$= -\left[RS_{k-1}^{k-1,v}\right] + Q^{k,v} \tag{3.42}$$

where

$$v = 0, 1, \ldots, v^k_{max}$$

and

$$k = 1, 2, \ldots, N$$

where v^k_{max} is the maximum number of sub–iteration in the kth outer iteration and N is the total number of Newton's iterations. The details of the logic are given in the flow chart in Fig. 3.1.

Exponential form of the relative permeability curves are used in this study (Sigmund and McCaffery, 1979). The following functions represent relative permeabilities to the non–wetting and wetting phases:

$$K_{rn} = K_{rn_e}\left(\frac{(S_{w_D})^{E_n} + A_n S_{w_D}}{1 + A_n}\right) \tag{3.43a}$$

$$K_{rw} = K_{rw_e}\left(\frac{(1 - S_{w_D})^{E_w} + A_w(1 - S_{w_D})}{1 + A_w}\right) \tag{3.43b}$$

where

$$S_{w_D} = \frac{S_w - S_{wir}}{1 - S_{or} - S_{wir}} \tag{3.43c}$$

This simulator along with the history matching package, described latter, is used to calculate relative permeability curves from displacement data. As this model takes into consideration the capillary forces, and the capillary end effect, the relative permeability curves obtained are free from errors caused by the capillary end effect. These curves are called *true relative permeability curves* in this study.

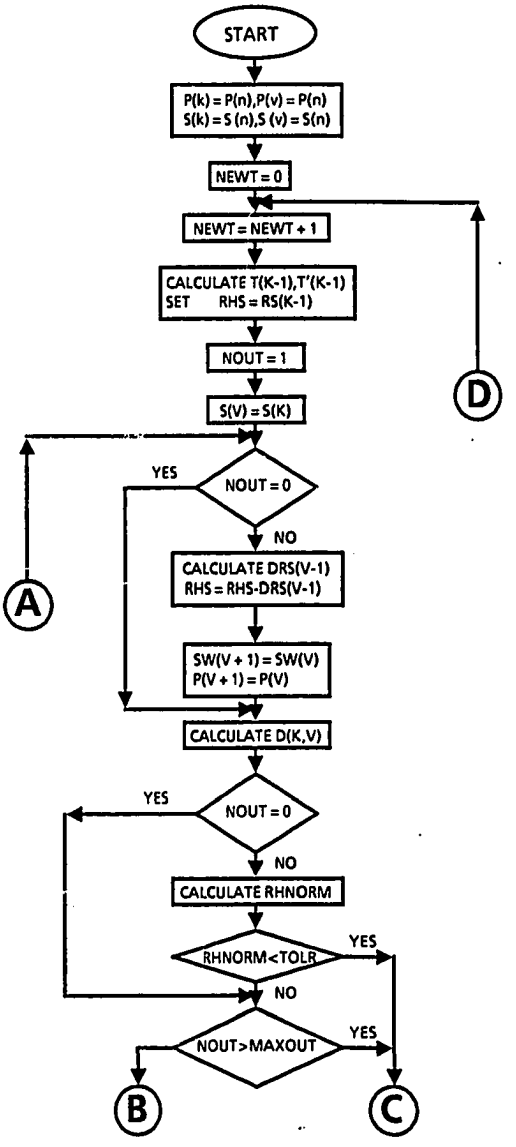

Fig. 3.1 Flow chart for each time step calculation of the numerical simulator

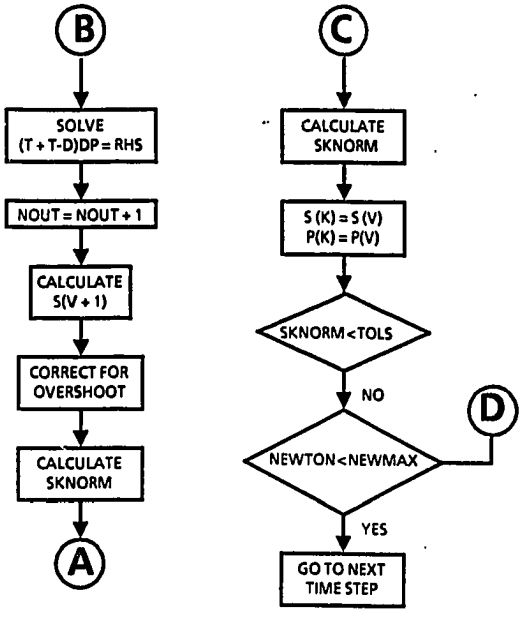

Fig. 3.1 Flow chart for each time step calculation of the numerical simulator (cont.)

3.2 THE NON-CAPILLARY WELGE MODEL

This model assumes that the capillary forces can be neglected during the displacement process. The calculation procedure can be divided into two parts. One is the calculation of recovery, and the other is the calculation of the pressure drop across the core. The details given here are for the case of water displacing oil. The calculations are similar for oil displacing water.

The calculation of the recovery from the core follows the approach presented by Welge(1952). For incompressible flow, the recovery from the core before water breakthrough is equal to the volume of water injected into the core. The recovery at any time after water breakthrough can be calculated from the difference between the average water saturation and the initial water saturation. The average water saturation after the breakthrough is given by (Welge, 1952);

$$\overline{S_w} = S_{w2} + \frac{q_t t}{A\phi L}(1 - f_{w2}) \tag{3.44}$$

and the slope of the fw curve at any time is given by;

$$f'_w = \frac{A\phi l}{q_t t} \tag{3.45}$$

The slope of the f_w curve calculated from equation (3.45)is used to find the saturation at the outlet end, (S_{w2}), and the corresponding fractional flow, f_{w2}. Equation (3.44) is used to calculate the average saturation, and hence the recovery at any time step.

To calculate the pressure drop across the core at any time, the concept of apparent total mobility is used (Willhite, 1986). The total flow rate q_t across

any cross-section of the core can be related to the pressure gradient at that cross-section by:

$$q_t = -\left(\frac{k_{ro}}{\mu_o} + \frac{k_{rw}}{\mu_w}\right) kA\frac{dp}{dx} \tag{3.46}$$

or

$$q_t = \lambda_r kA\frac{dp}{dx} \tag{3.47}$$

where

$$\lambda_r = \frac{k_{ro}}{\mu_o} + \frac{k_{rw}}{\mu_w} \tag{3.48}$$

Separating the variables and integrating equation 3.46 we get:

$$\Delta p = \frac{q_t \int_0^L \lambda_r^{-1} dx}{kA} \tag{3.49}$$

To find the pressure drop across the core, we need to evaluate the integral on the right hand side of equation 3.48. We can define the average apparent viscosity for the linear system over a distance L as:

$$\overline{\lambda^{-1}} = \frac{\int_0^L \lambda_r^{-1} dx}{\int_0^L dx} \tag{3.50}$$

Writing the Buckley–Leverett equation as;

$$\left(\frac{dx}{dt}\right)_{S_w} = \frac{q_t}{\phi A}\left(\frac{\partial f_w}{\partial S_w}\right)_t \tag{3.51}$$

and after separating the variables and integrating, we get :

$$\int_0^{x_{sw}} dx = \int_0^t \left(\frac{q_t}{A\phi}\right) f'_{S_w} dt \tag{3.52}$$

where we have used the definition

$$f'_{S_w} = \left(\frac{\partial f_w}{\partial S_w}\right)_{S_w} \tag{3.53}$$

Now we define:

$$Q_i = \frac{\int_0^t q_t dt}{V_p} \tag{3.54}$$

So that equation (3.52) can be written as:

$$x_{s_w} = LQ_i f'_{s_w} \tag{3.55}$$

When Q_i is fixed x_{s_w} is a function of f'_{s_w} only, x_{s_w} and x are identical so that equation 3.54, after differentiation, can be written as:

$$dx = LQ_i df'_{s_w} \tag{3.56}$$

Substituting this term into 3.55 and simplifying, we get:

$$\frac{\int_0^L \lambda^{-1} dx}{\int_0^L dx} = \frac{\int_0^{f'_{s_{w2}}} \lambda_r^{-1} df'}{f'_{s_{w2}}} \tag{3.57}$$

where $f'_{S_{w2}}$ is the derivative of the fractional flow curve at $x = L$. After breakthrough $\overline{\lambda^{-1}} = \overline{\lambda_2^{-1}}$. Thus (3.50) gives

$$\overline{\lambda_2^{-1}} = \frac{\int_0^{f'_{S_{w2}}} \lambda_r^{-1} df'_{S_w}}{f'_{S_{w2}}} \tag{3.58}$$

After evaluating $\overline{\lambda_2^{-1}}$ for any saturation greater than the front saturation, equation 3.49 can be used to calculate pressure drop across the core at any time after the breakthrough time. For the interval before breakthrough the integral in equation 3.49 is written as the sum of two integrals.

$$\int_0^L \lambda_r^{-1} dx = \int_0^{x_{s_{wf}}} \lambda_r^{-1} dx + \int_{x_{s_{wf}}}^L \lambda_r^{-1} dx \tag{3.59}$$

$$\int_0^{x_{s_{wf}}} \lambda_r^{-1} dx = x_{s_{wf}} \overline{\lambda_{s_{wf}}^{-1}} \tag{3.60}$$

This equation along with equation 3.49 is used to calculate the pressure drop across the core before breakthrough.

This Welge model can be used to simulate two phase flow that neglects capillarity. When used with the history matching package to calculate relative permeabilities, this gives curves which are in error because we have neglected the capillary end effect. Because we use the parametric form of the relative permeability curves, this model gives curves which are defined over the entire saturation range. Therefore, the exponents and the end point relative permeabilities can be compared to their true values given by the numerical simulator.

3.3 HISTORY MATCHING PACKAGE

For history matching purpose we define a least squares objective function as the sum of the squares of the normalized differences between the observed and calculated recovery and pressure drop at each time step. Mathematically this can written as:

$$J(K_{rw_e}, K_{rn_e}, E_w, E_n) = \sum_{i=1}^{N} \left[\frac{\Delta p_{obs} - \Delta p_{cal}}{\Delta p_{init}} \right]^2 + \sum_{i=1}^{N} \left[\frac{R_{obs} - R_{cal}}{R_t} \right]^2 \quad (3.62)$$

The objective function J is minimized using a Levenberg–Marquardt algorithm. In this minimization process the parameters K_{rw_e}, K_{rn_e}, E_w, and E_n are allowed to change until a minimum of the objective function is found.

If we use the following definitions,

$$Y_p = \left(\frac{\Delta p_{obs} - \Delta p_{cal}}{\Delta p_{init}} \right) \quad (3.63)$$

$$Y_R = \left(\frac{R_{obs} - R_{cal}}{R_t} \right) \quad (3.64)$$

and

$$\vec{\mathbf{X}} = [K_{rw_e}, K_{rn_e}, E_w, E_n] \tag{3.65}$$

then the objective function becomes

$$J(\vec{\mathbf{X}}) = \sum_{i=1}^{N} (Y_p^2 - Y_R^2) \tag{3.66}$$

Applying the Levenberg-Marquardt method to the objective function given by equation (3.66) the search direction $\mathbf{S}$, can be defined (Reklaitis et al,1983):

$$\mathbf{S}(\vec{\mathbf{X}}^k) = -[\mathbf{H}^k + \lambda^k \mathbf{I}]^{-1} \nabla J(\vec{\mathbf{X}}^k) \tag{3.67}$$

where $\mathbf{I}$ is the identity matrix and $\mathbf{H}$ is the Hessian matrix. The element of the Hessian matrix in the ith row and jth column is given by:

$$h_{ij} = \frac{\partial^2 J}{\partial x_i \partial x_j} \tag{3.68}$$

and the Hessian matrix $\mathbf{H}$ is:

$$H = \begin{pmatrix} \frac{\partial^2 J}{\partial x_1^2} & \frac{\partial^2 J}{\partial x_1 \partial x_2} & \frac{\partial^2 J}{\partial x_1 \partial x_3} & \frac{\partial^2 J}{\partial x_1 \partial x_4} \\ \vdots & \vdots & \vdots & \vdots \\ \frac{\partial^2 J}{\partial x_4 \partial x_1} & \frac{\partial^2 J}{\partial x_4 \partial x_2} & \frac{\partial^2 J}{\partial x_4 \partial x_3} & \frac{\partial^2 J}{\partial x_4^2} \end{pmatrix} \tag{3.69}$$

In equation (3.67), λ is the Marquardt's parameter, which controls the direction and step length of the search. When λ approaches $+\infty$, the Marquardt's method reduces to the method of steepest descent. When λ is equal to zero, the method is equivalent to the Gauss-Newton (Kuester and Mize, 1973; Reklaitis et al, 1983; Fletcher, 1980).

The gradient vector $\vec{\nabla \mathbf{J}}$ is defined as:

$$\vec{\nabla \mathbf{J}} = \begin{pmatrix} 2\sum_{i=1}^{n} [Y_p \frac{\partial Y_p}{\partial x_1} + Y_R \frac{\partial Y_R}{\partial x_1}] \\ 2\sum_{i=1}^{n} [Y_p \frac{\partial Y_p}{\partial x_4} + Y_R \frac{\partial Y_R}{\partial x_4}] \end{pmatrix} \tag{3.70}$$

If we define:

$$\vec{A} = \nabla \vec{J}(\vec{X}^k) \tag{3.71}$$

the Hessian matrix $\mathbf{H}$ can be approximated by $\vec{A}\vec{A}^T$ (Fletcher, 1980). This approximation is advantageous from computational point of view. With this approximation equation (3.67) can be written as:

$$\mathbf{S}(\vec{X}^k) = -[\vec{A}\vec{A}^{Tk} + \lambda^k \mathbf{I}]^{-1} \tag{3.72}$$

The gradient vector $\vec{A}$ is found in this study by numerical differentiation. The flow chart for the history matching algorithm is given in Fig. 3.2.

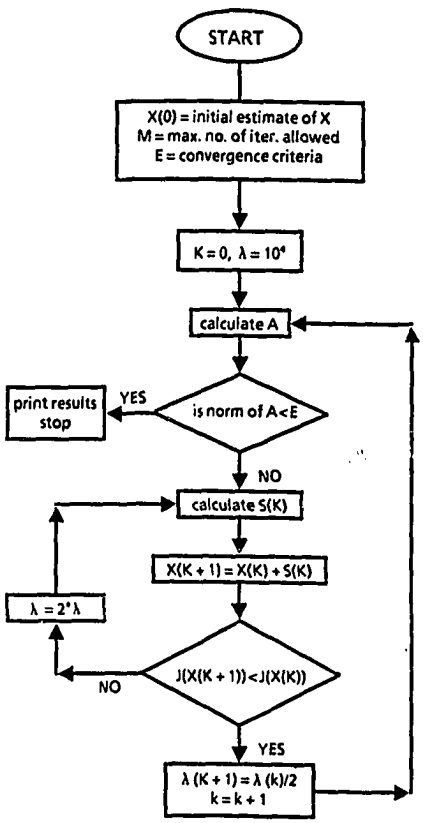

Fig. 3.2 Flow chart for the Levenberg–Marquardt algorithm

4. EXPERIMENTAL SETUP AND PROCEDURE

This chapter is divided into two sections. The details of the experimental setup are given in the first section. The experimental procedure is described in the second section.

4.1 EXPERIMENTAL SETUP

As part of this study an experimental setup was designed and constructed to perform displacement studies on consolidated core samples. It is possible to conduct both steady state and displacement type experiments on one inch diameter and up to ten inch long core samples, under controlled temperature and pressure conditions. To ensure that changes in the ambient temperature do not affect the measurements, the core holder is mounted inside a constant temperature air bath. The temperature of the bath can be maintained within $\pm 0.2^{\circ}$ C of the set temperature by continuously circulating cold water through a radiator, and by an electric heater which is controlled by an electronic controller. The experimental setup is shown in Figure 4.1. Using this setup, flow experiments can be conducted either using continuous or recirculation flow system by switching over appropriate valves. The main components of the setup are described in the following sections.

4.1.1 Pumps

The pumps used in this study are model FDS-220 and FDS-210, manufactured by Petrophysical Services in Mountain View, California. These pumps are positive displacement dual cylinder pumps. The pump motors are controlled

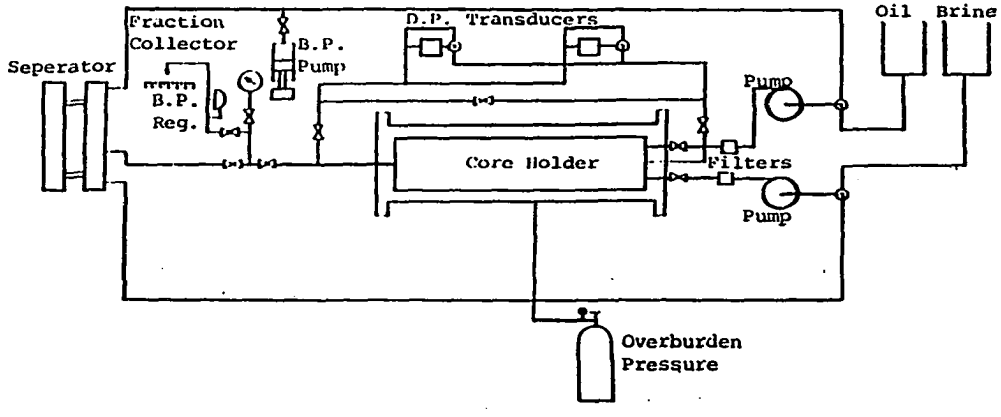

Figure 4.1 Schematic of the experimental setup for measuring relative permeabilities.

by microprocessors. The pumps can be operated either in constant flow rate or constant pressure mode. In the constant flow rate mode the pumps can either operate in smooth or geared mode. In the smooth mode the pressure fluctuations at the switching of flow from the cylinders are minimized and in the geared mode the pump simulates a dual piston mechanical pump. The FDS–220 has two pumps built in a single unit. One pump in this unit is used to inject brine, and the other is used to inject oil into the core. The FDS–210 was used to maintain a constant back pressure in the system in experiments involving recirculaion of the fluids.

4.1.2 Core Holder

The core holder used in these experiments was a model RCH–10–3 , from Temco, Tulsa, Oklahoma. This core holder was modified so that the mixing of the fluids in steady state experiments occurs as close as possible to the core face. The pressure taps on either end of the core were also moved closer to the core faces, thus eliminating the error caused by the extra pressure drop in the flow lines. This core holder can hold one inch diameter and up to ten inch long cores inside a viton sleeve. Overburden pressure is applied around this sleeve to stop leakage of fluids around the core. The overburden pressure was at all times maintained 400 psi greater than the system pressure. The core holder can be operated up to an overburden pressure of 2500 psi, and a maximum temperature of 350° F.

4.1.3 Separator

The separator was used to separate and monitor the material balance in the system, so that the saturation of the fluids in the core can be determined at any time. The separator used was a model AMS–780 from Litton Core Research, Mountain View, California. This separator can be operated up to a pressure of 10,000 psi and a temperature of 300° F. The height of the interface in this separator is calculated by measuring the time of travel of acoustic pulses from the bottom of the separator to the oil–brine interface. The height is converted to the volume of brine in the separator by multiplying the height with the cross–sectional area. The volumes can be measured with an accuracy of ±0.1 cc. The control unit of the separator does all the necessary calculations, and the final volume is transmitted to a personal computer for real–time recording. The separator is continuously calibrated by measuring the travel time of the acoustic pulses to a fixed ring inside the separator.

4.1.4 Differential Pressure Transducers

To measure the pressure drop across the core, four model DP–15 differential pressure transducers along with CD–18 carrier demodulators in an MC1–333 module case were used. These are manufactured by Validyne Engineering Corporation of Northridge, California. To accurately measure widely varying pressure drop, four different transducers were used, with pressure drop ranges of: 0–5, 0–20, 0–80, and 0–300 psi. At any one time two transducers were installed in the system. But provision was made to replace the transducers in the system with minimum

disturbance to the experiment. The carrier demodulator supplied the carrier voltage to the transducer and converted the signal from transducer to a voltage signal of 0–10 volts dc. This voltage signal was recorded on a Fisher Recordall series 5000 chart recorder. The other pen of the chart recorder was used to record the temperature of the air bath. The overall accuracy of each differential pressure transducer is 1% of the full scale.

4.1.5 Back Pressure Regulator

In case of continuous flow experiments a dome type back pressure regulator was used to maintain the necessary system pressure. The back pressure regulator used was model 91W Mity Mite manufactured by Grove Valve and Regulator Company, California. This regulator is capable of maintaining a back pressure of 100–2000 psi on the system. All the lines used in the system were 1/8th inch monel tubing. The valves and fittings were all stainless steel. The filters used were two micron stainless steel for oil and seven micron monel for the brine.

4.2 EXPERIMENTAL MATERIALS AND PROCEDURE

This section describes the materials used for the study and the experimental procedure. The core samples used were from Berea quarry. Three cores of one–inch diameter and different lengths were used for these experiments. The dimensions and properties of these cores are given in Table 4.1

Table 4.1: Properties of core samples

	Length (cm)	Absolute Permeability (md)	Porosity %
Core No. 1	24.1	528	24.4
Core No. 2	25.4	980	22.8
Core No. 3	12.7	950	23.0

The fluids used in the experiments were 2% NaCl brine and depolarized kerosene. The brine used was de-aerated by vacuum. The kerosene oil was depolarized by passing through a silica gel column. The experimental procedure is given in detail in the following paragraphs.

4.2.1 Sample Preparation

The first step in each experiment was to prepare the core sample. The one-inch diameter cores were cut from a block of sandstone obtained directly from the quarry. The core was cut to the required length with a diamond saw. To avoid the problem of clays swelling during the experiment, the cores were fired in a furnace at 400°C for twelve hours. After the core sample cooled down to the room temperature, it was wrapped in teflon tape to avoid the prolonged contact of the fluids with the sleeve. The core was then mounted in the core holder for the determination of porosity.

4.2.2 Porosity Determination

Porosity of the each core sample used was measured by using Boyle's law. The schematic of the set up used is shown in Figure 4.2. The buret is filled to the top with water. With valve–2 closed the core is pressurized by opening valve–1. After valve–1 is closed, the system is allowed to equilibrate. The pressure in the system is measured using the pressure gauge. As valve–2 is opened the gas expands into the buret and the system pressure drops to atmospheric pressure. The volume of gas produced into the buret V_g is noted. If P_g is the pressure before expansion, P_{bar} is the barometric pressure and h is the height of water in the buret from the free water level in the beaker, equation (4.1) gives the volume of the system V_s, between valves 1 and 2. That is:

$$V_s = \frac{V_g(P_{bar} - \rho_w g h)}{P_g} \tag{4.1}$$

By repeating the experiment without the core, the dead volume of the system can be determined. Subtracting the dead volume from the total volume obtained above gives the pore volume of the core, V_p. The porosity can be calculated from equation:

$$\phi = \frac{V_p}{V_b} \tag{4.2}$$

where the bulk volume V_b is calculated from the length and the diameter of the core. After the determination of the porosity the next step is the saturation of the core. the procedure is described in the next paragraph.

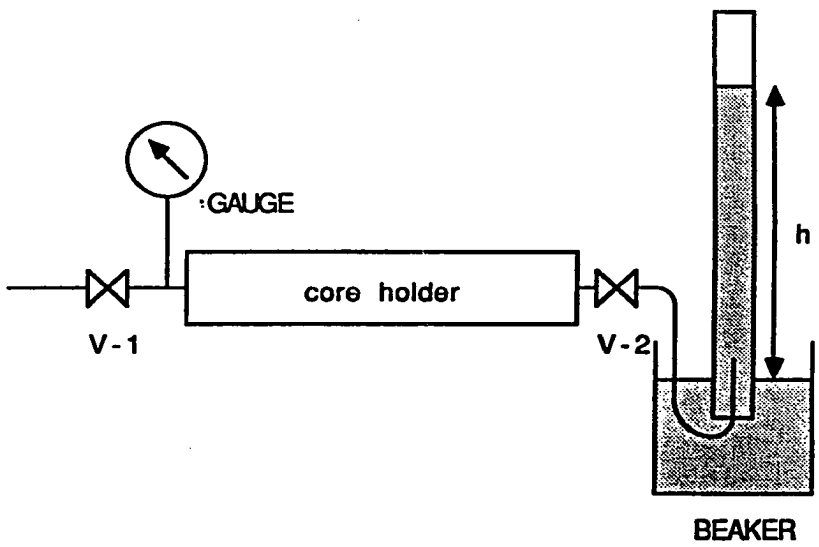

Fig. 4.2 Schematic of the experimental setup for measuring porosity

4.2.3 Saturation Determination

To ensure that the core is fully saturated with the brine, the following steps are taken:

1- The core is flooded with carbon dioxide at a low rate for the displacement of air. Since carbon dioxide is soluble in brine, any traces of it are easily removed from the core by flowing the brine through the core.

2- After complete displacement of air the core is placed under vacuum for twenty four hours.

3- Deaerated brine is allowed to imbibe the core under atmospheric pressure. After removing the vacuum lines the core holder is placed in the system and brine is pumped through the core at a rate of 2 cc/min under a back pressure of 500 psi. This high back pressure forces any traces of gas trapped in the core to be dissolved in the brine and thus flow of it. The flow of brine also causes the clay minerals to stabilize. The flow of brine is continued until the pressure drop across the core has stabilized. At this stage the absolute permeability of the core can be determined.

4.2.4 Determination of the Absolute Permeability

To measure the absolute permeability of the core, brine is pumped through it at different rates and the stabilized pressure drop corresponding to each rate is

recorded. The ratio of the flow rate to the pressure drop is determined by fitting a straight line through the data points. Absolute permeability can be calculated by applying Darcy's law. That is,

$$k_{abs} = \frac{\mu L}{A}\left(\frac{Q}{\Delta P}\right) \tag{4.3}$$

After the determination of the absolute permeability the core is ready for relative permeability experiments.

4.2.5 Relative Permeability Determination

The first step in determining the relative permeability is the primary drainage process. Oil at 2 cc/min is injected through the core to bring it to the irreducible water saturation. After this either steady–state or displacement experiments can be conducted to determine the relative permeability curves.

4.2.5.1 Steady State Experiments

Steady state experiments were conducted on core no. 1 to validate the simulator along with the history matching package. In these experiments brine and oil are injected into the core at different brine–oil ratios, keeping the total flow rate constant at 2 cc/min. After the pressure drop and the saturation stabilize for a period of 6 hours, the pressure drop and saturation are recorded. The pressure drop and the flow rate are used in the Darcy's law to calculate the effective permeabilities for each phase at that particular saturation. The imbibition curve

is traced by increasing the brine–oil ratio in steps from zero to one. By decreasing the ratio from one to zero the drainage curve can be traced.

4.2.5.2 Displacement Experiments

In displacement experiments only one of the fluids is injected into the core, the pressure drop and the recovery data from the core are continuously recorded. To obtain the imbibition curve only brine is injected, while for the drainage curve only oil is injected into the core. After each low flow rate run (less than 2 cc/min), the flow rate was increased to 2 cc/min until production of the displaced phase from the core stopped. This was done to ensure that the core is at the same initial condition at the beginning of each run. The data from the displacement runs was analyzed with the history matching package using either the numerical simulator for true relative permeabilities or using the Welge type model for the relative permeabilities in error due to the capillary end effects. Both of these models were validated as discussed in the next chapter. To use the displacement data with the numerical simulator, reliable capillary pressure data was required. This data was obtained by a Beckman centrifuge using modified drainage buckets described in the next section.

4.2.6 Capillary Pressure Measurements

The centrifuge can be used to measure the capillary pressure curves in a short time. The disadvantage of this method was that it is not possible to

determine the imbibition capillary pressure curve for strongly water wet core. This problem was solved by a simple modification of the standard drainage bucket as shown in Figure 4.3.

A semi-permeable plate was placed under the core. A capillary tube was attached to this plate, the other end of which was in the brine at the bottom of the collection tube. Both the plate and the capillary tube assembly were saturated with brine under vacuum before putting them in the bucket. The drainage curve was traced by the conventional method of increasing the centrifuge speed in steps and measuring the production from the core. At the end of the drainage cycle the speed of the centrifuge was reduced in steps. As the capillary pressure in the core decreased, water was able to imbibe back through the capillary tube and the semi-permeable plate. The imbibition of brine into the core was recorded at each step to calculate the imbibition curve.

Steady state and displacement experiments were conducted on three core samples. The displacement data from these experiments were analyzed to calculate the relative permeability curves using the software described in the last chapter. These procedures were verified by comparing these curves with the steady state data. The raw data from these experiments is presented in the appendix. The results of this study are discussed in detail in the next chapter.

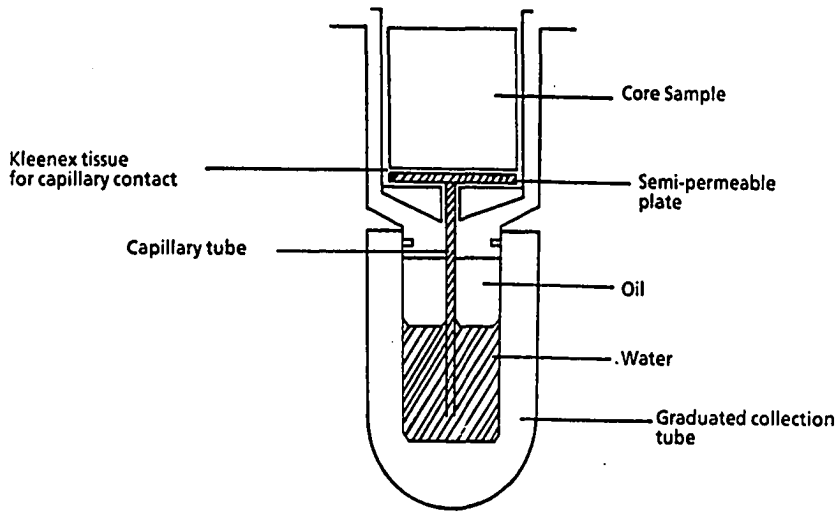

Fig. 4.3 Modified drainage capillary pressure bucket for measuring both imbibition and drainage capillary pressure curves

5. RESULTS AND DISCUSSION

The results obtained by analyzing the raw data as obtained by the experimental procedures described in the last chapter are discussed in this chapter. To use the numerical simulator as a model of core floods for history matching requires reliable drainage and imbibition capillary pressure curves. These capillary pressure curves were obtained by using the modified drainage centrifuge bucket described at the end of the last chapter. The imbibition and drainage curves are shown in Figure 5.1.

The experimental data from core # 1 was used to validate the models and the history matching package. After validation the data was used to generate the correlations. The data from cores # 2 and # 3 was used to check the validity of the correlations developed. Table 5.1 through 5.3 show the flow rates at which the experiments were conducted on cores # 1 through # 3 respectively. The saturations and the end point relative permeabilities measured at the end of each experiment are also shown in these tables.

For core # 1 the first displacement (primary drainage) is conducted at a rate of 2 cc/min. This is followed by 1 cc/min displacement runs and subsequently 0.5 cc/min. runs. The steady state experiments were conducted at 2 cc/min cumulative flow rate after the displacement experiments. The validation of the software and results are discussed both for drainage and imbibition in the following paragraphs.

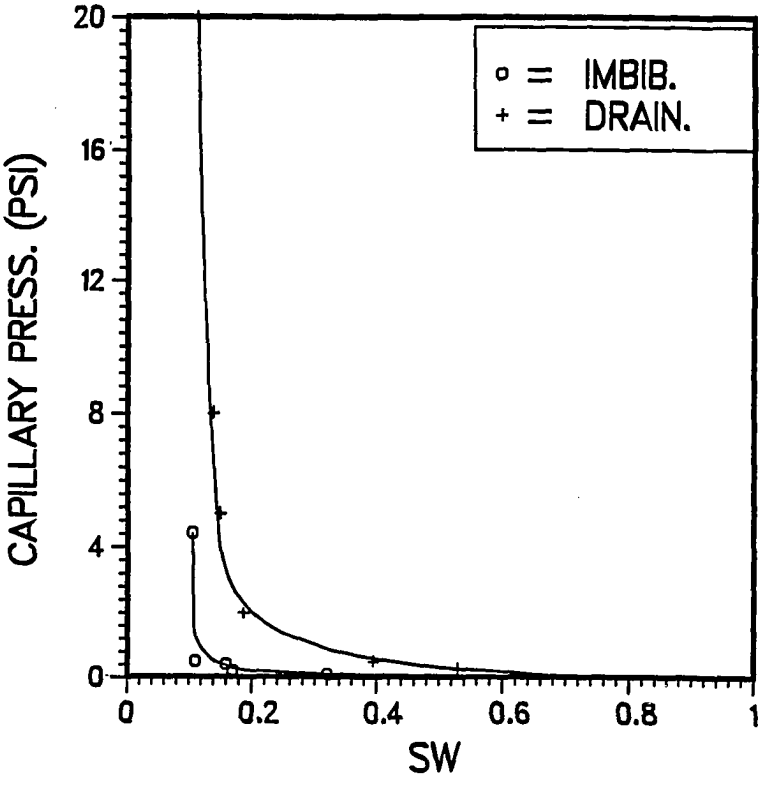

Fig. 5.1 Drainage and imbibition capillary pressure data measured on Berea sand stone core.

Table 5.1: Displacement experiments conducted on core # 1

K_{abs} = 528 md ϕ = 24% Length = 24.1 μ_w = 0.93 cp μ_{nw} = 1.50 cp

Experiment No.	Experiment Type	Rate cc/min	$S_{w(end)}$ After Bump	$Kr_{w(end)}$	$Kr_{o(end)}$	Average S_w Before Bump
1	Displacement Primary Drainage	2	0.23	---	0.822	---
2	Displacement Imbibition	1	0.67	0.058	---	---
3	Displacement Drainage	1	0.27	---	0.635	0.32
4	Displacement Imbibition	1	0.66	0.053	---	0.65
5	Diplacement Drainage	0.5	0.28	---	0.661	0.37
6	Displacement Imbibition	0.5	0.65	0.046	---	0.64
7	Steady State Drainage	2	0.28	---	0.69	---
8	Steady State Imbibition	2	0.69	0.04	---	---

Table 5.2: Displacement experiments conducted on core # 2

K_{abs} = 980 md ϕ = 23% Length = 25.4 μ_w = 0.93 cp μ_{nw} = 1.50 cp

Experiment No.	Experiment Type	Rate cc/min	$S_{w\,(end)}$ After Bump	$Kr_{w\,(end)}$	$Kr_{o\,(end)}$	Average S_w Before Bump
1	Primary Drainage	2	0.20	---	0.72	---
2	Imbibition	2	0.63	0.174	---	---
3	Drainage	2	0.21	---	0.72	---
4	Imbibition	1	0.60	0.085	0.725	0.60
5	Drainage	1	0.19	---	0.721	0.22

Table 5.3: Displacement experiments conducted on core # 3

K_{abs} = 950 md Φ = 23% Length = 25.4 μ_w = 0.93 cp μ_{nw} = 1.50 cp

Experiment No.	Experiment Type	Rate cc/min	$S_{w(end)}$ After Bump	$Kr_{w(end)}$	$Kr_{o(end)}$	Average S_w Before Bump
1	Primary Drainage	2	0.14	---	0.72	---
2	Imbibition	2	0.55	0.077	---	---
3	Drainage	0.2	0.13	---	0.625	0.27

5.1 DRAINAGE

The data obtained from the experiment no. 3 of core # 1 were used to obtain the *true drainage relative permeability* curves (free from capillary end effects). The experimental recovery and pressure drop data are shown in Figure 5.2.

The simulated data at the end of the history match are also shown in the same figure for comparison. Both curves show a very good match except for the early time data, which are very difficult to obtain in the experiment. In all of these experiments the pressure drop across the core is measured with an accuracy of ± 0.8 psi. The recovery data are accurate within ± 0.1 c.c. The true relative permeability curves along with the steady-state curves from the same core are shown in Figure 5.3. As can be seen from Figure 5.3, the curves show a good match. The end point relative permeability for the non-wetting phase measured during the steady state experiments is lower than that obtained from the displacement experiment. This is because of the different flow mechanisms operating in the displacement and the steady state flow processes, as reported by Handy and Data(1966).

For further validation of the model, the recovery and the pressure drop data for an injection rate of 0.5 cc/min. were generated using the finite difference simulator and compared with the experimental data obtained in experiment no. 5 on core # 1. The two sets are in very good agreement as shown in Figure 5.4.

After the validation of the simulator and the history matching algorithm, the recovery and pressure drop data were generated using the true relative permeability curves in the simulator, for flow rates of 0.2, 0.1, 0.05 cc/min. The 0.2

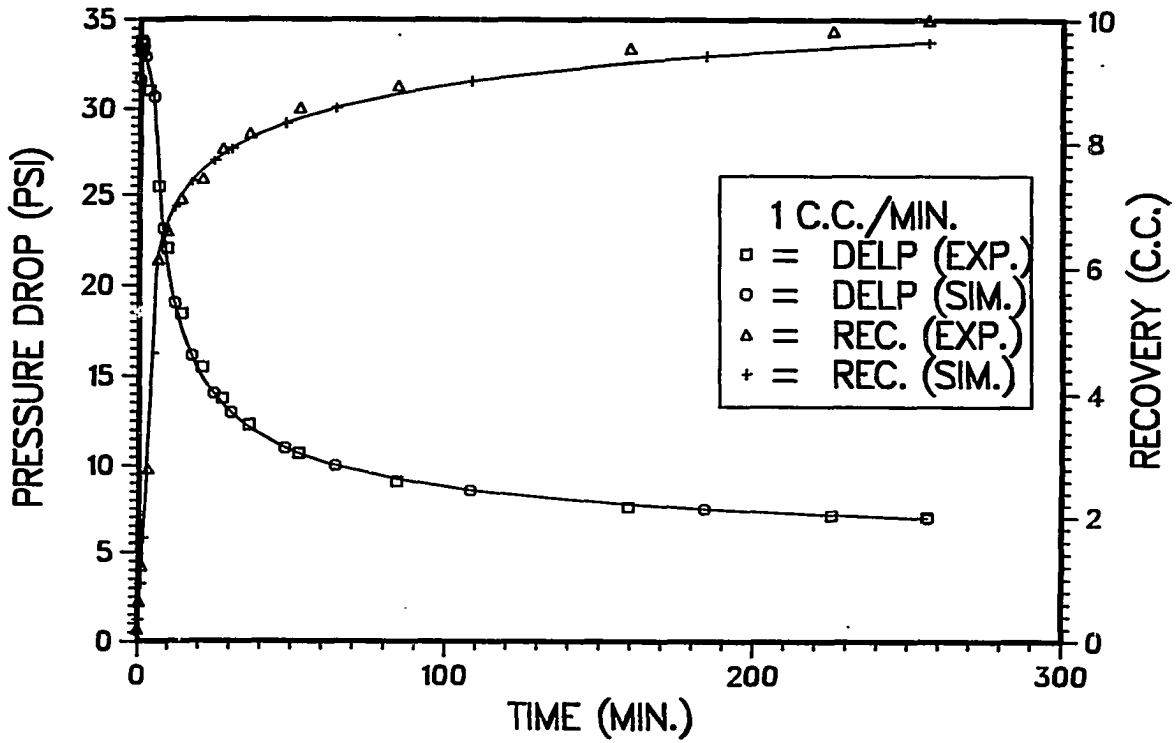

Fig. 5.2 Experimental and simulated recovery and pressure drop data for 1.0 cc/min. drainage run on core # 1.

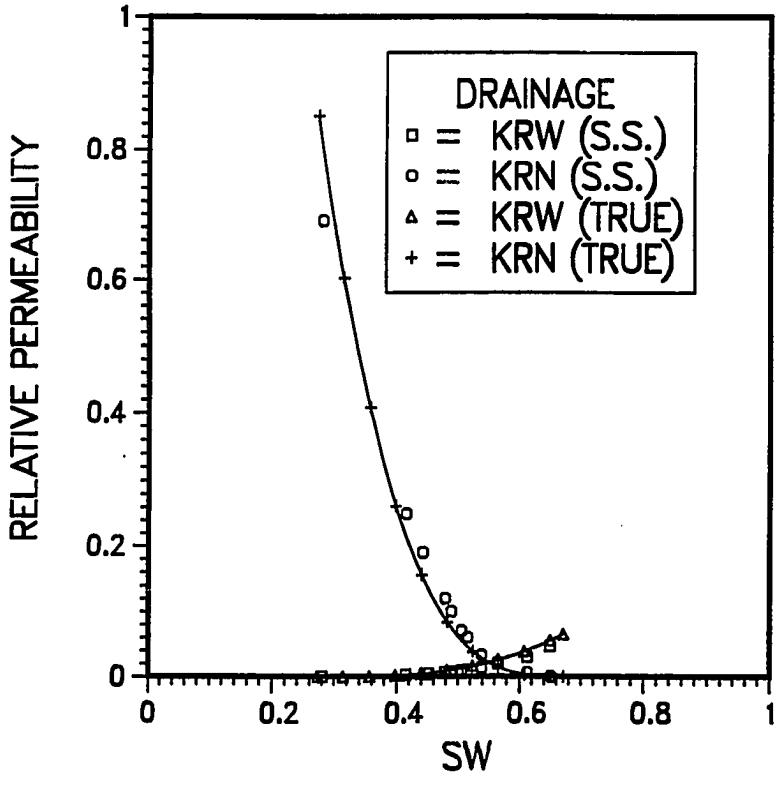

Fig. 5.3 Comparison of steady state and true drainage relative permeability curves for core # 1.

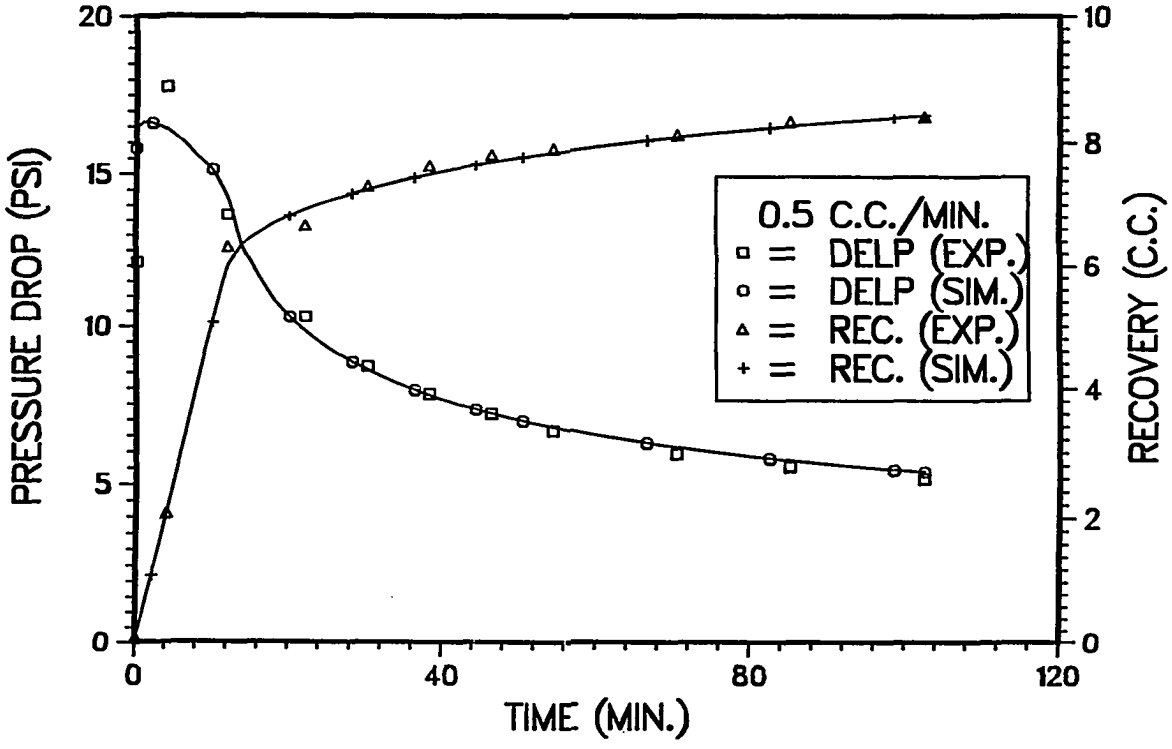

Fig. 5.4 Experimental and simulated recovery and pressure drop data for 0.5 cc/min. drainage run on core # 1.

cc/min. simulated data were analyzed by both the JBN and the history matching algorithm with Welge type model. The results are compared in Figure 5.5. The curve generated by history matching falls on the data points generated by JBN, but covers a much broader range of saturations, which is advantageous. After this validation, the recovery and pressure drop data from simulated low rate runs were used to find the parameters of the equations describing the relative permeability curves. These relative permeability curves are in error because the capillary forces are neglected in the model, hence we call them *false* relative permeability curves. The *false* relative permeability curves along with the *true* curves are presented in Figure 5.6. The decrease in the relative permeabilities with a decrease in the rate shows a definite trend.

Since the relative permeability curves are defined by the four parameters E_n, E_w, $K_{rn_{end}}$, and $K_{rw_{end}}$, the change in the relative permeabilities with rate can now be quantified with the change in these parameters. The changes in these parameters are presented in Figures 5.7, through 5.10 as functions of the dimensionless rate, defined by:

$$R_D = \frac{L\mu q}{Ak\left(\frac{\sigma}{\sqrt{K/\phi}}\right)} \tag{5.1}$$

The abscissa in all of these figures is this dimensionless rate and the ordinate is the ratio of the *false* to *true* parameter.

Regression equations derived both in the exponential and polynomial forms were fit to the curves plotted in Figures 5.7 through 5.10 to find the functional form of the change of each parameter with dimensionless rate. The following are

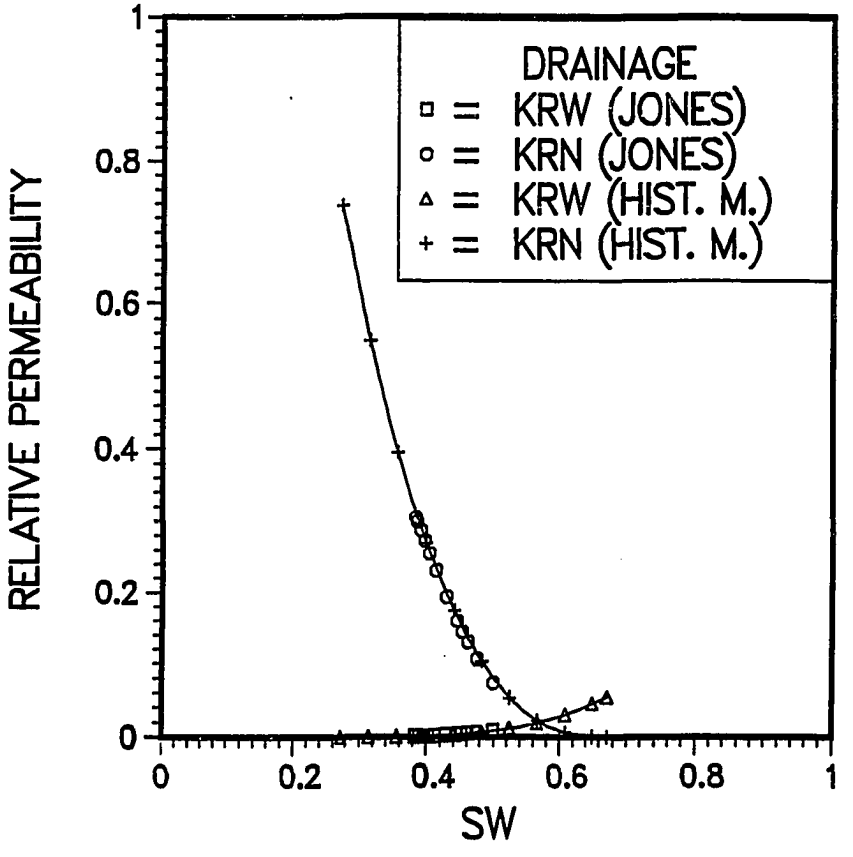

Fig. 5.5 Comparison of relative permeability curves generated by history matching and Jones and Rozelle method.

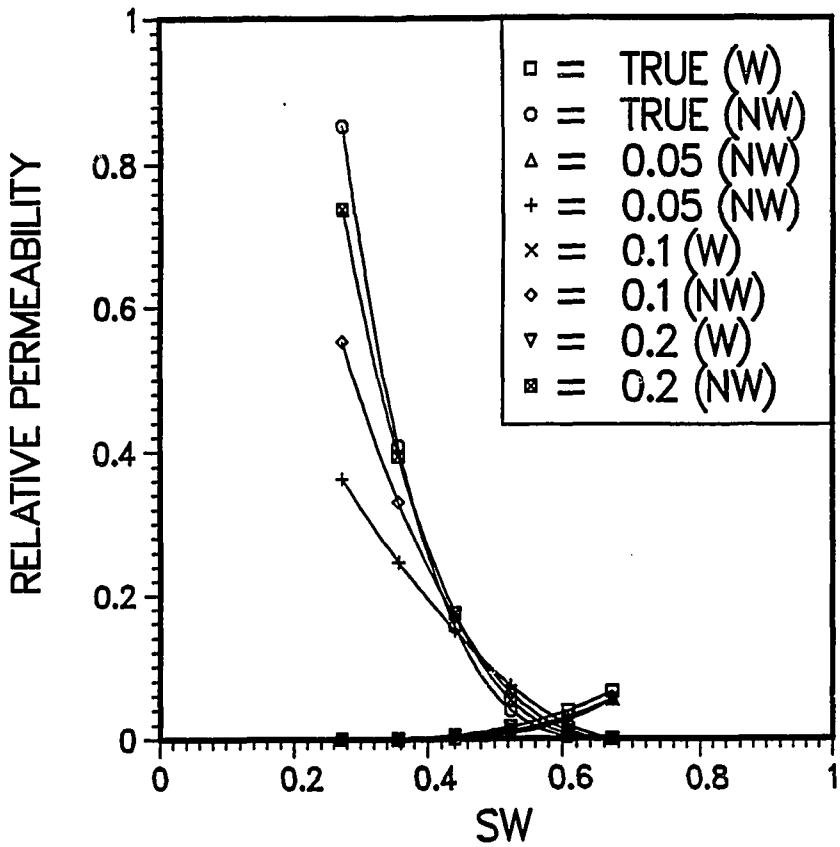

Fig. 5.6 True and false relative permeability curves for different rates.

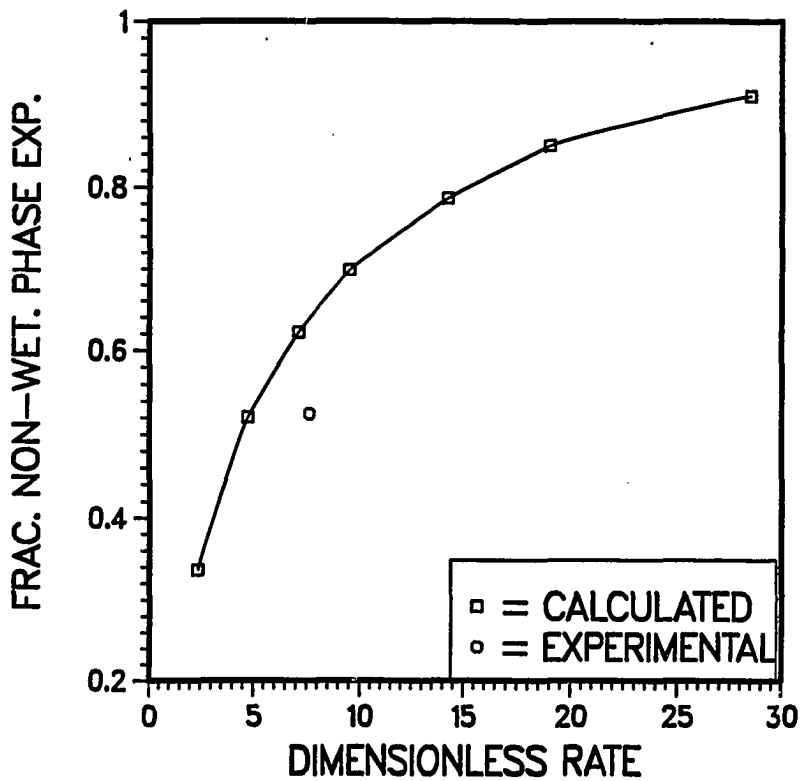

Fig. 5.7 Ratio of true to false non-wetting phase exponents vs dimensionless rate.

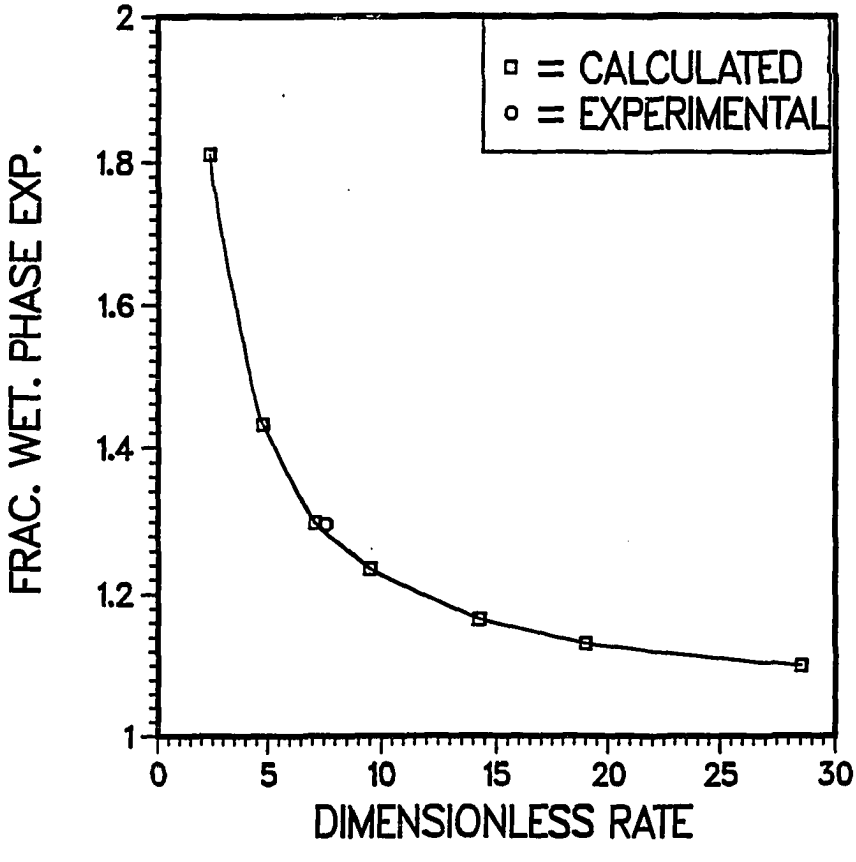

Fig. 5.8 Ratio of true to false wetting phase exponents vs dimensionless rate.

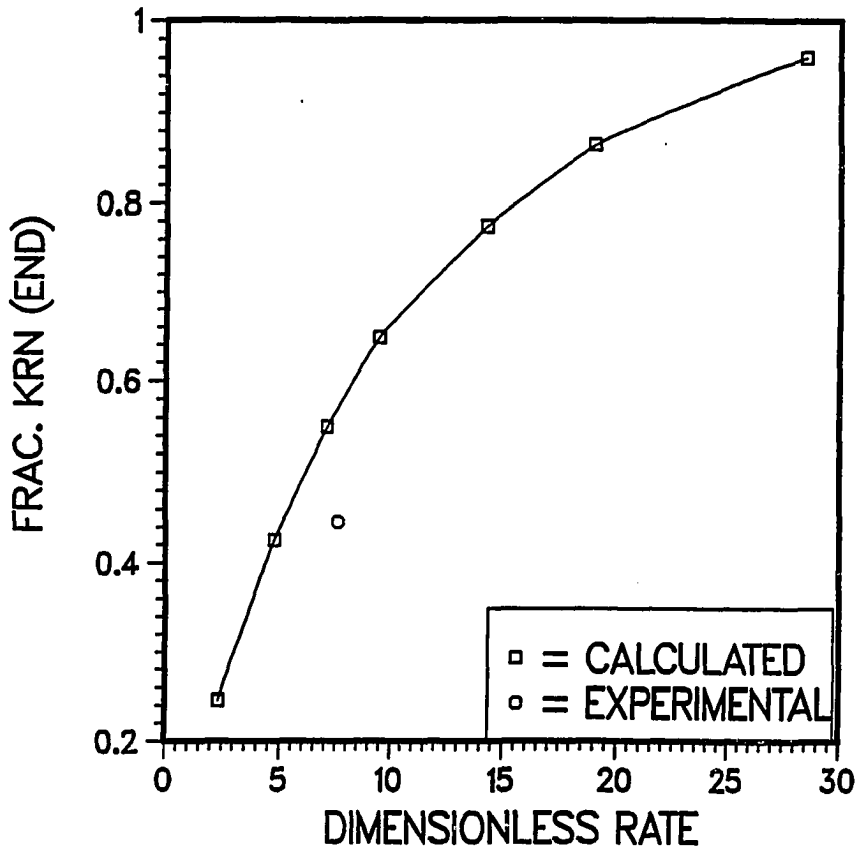

Fig. 5.9 Ratio of true to false end point non-wetting phase relative permeability vs dimensionless rate.

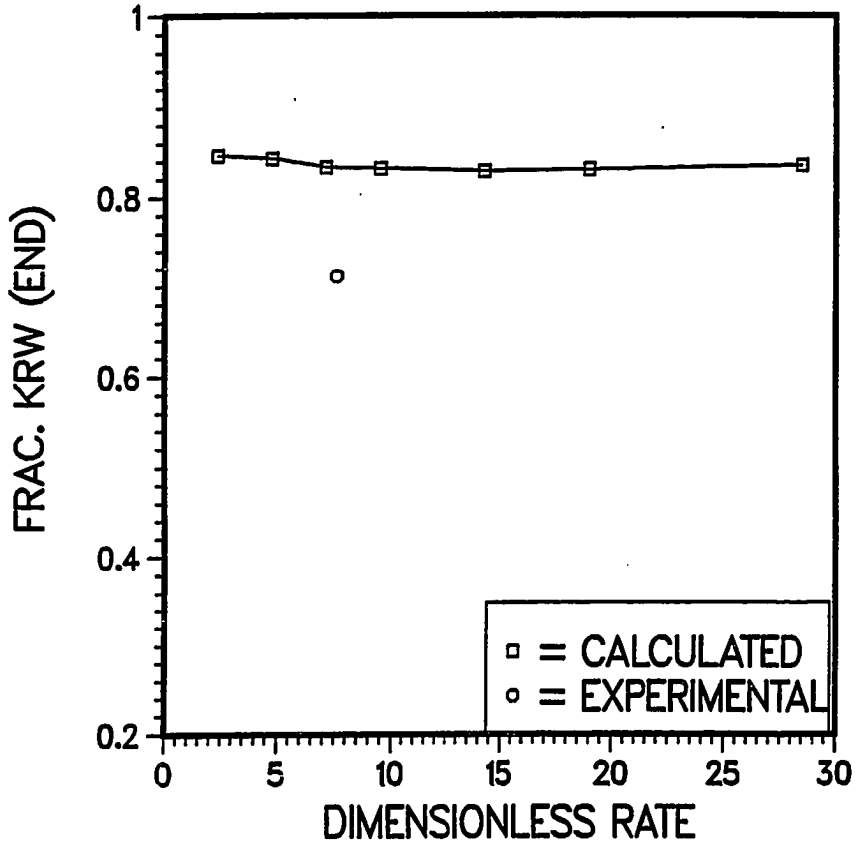

Fig. 5.10 Ratio of true to false end point wetting phase relative permeability vs dimensionless rate.

the exponential forms:

$$\frac{k_{rn_{end}}}{(k_{rn_{end}})_{true}} = 0.188 - 1.4 \times 10^{-5} exp(R_D/2) + 0.045 R_D \tag{5.2}$$

$$\frac{E_n}{(E_n)_{true}} = 0.308 - 1.4 \times 10^{-5} exp(R_D/2) + 0.038 R_D \tag{5.3}$$

and

$$\frac{E_w}{(E_w)_{true}} = 1.28 + 1.8 exp(-R_D/2) - 0.0071 R_D \tag{5.4}$$

The exponential form was not applicable to the ratio of the wetting phase end point relative permeability to its *true* value.

The polynomial forms are:

$$\frac{k_{rn_{end}}}{(k_{rn_{end}})_{true}} = 0.140 + 0.062 R_D - 1.2 \times 10^{-3} R_D^2 \tag{5.5}$$

$$\frac{k_{rw_{end}}}{(k_{rw_{end}})_{true}} = 0.85 - 0.0025 R_D - 7 \times 10^{-5} R_D^2 \tag{5.6}$$

$$\frac{E_n}{(E_n)_{true}} = 0.705 - 0.95 R_D^{-1} + 9 \times 10^{-4} R_D \tag{5.7}$$

$$\frac{E_w}{(E_w)_{true}} = 1.04 + 1.82 R_D^{-1} - 4.6 \times 10{-}4 R_D \tag{5.8}$$

To investigate the applicability of these functions to other cores, the displacement experiments in other core samples were analyzed. Core # 2 and # 3 were taken from the same outcrop with the same approximate permeability as core #1. It is assumed that the capillary effects in the 2 cc/min. run from core # 2, which is the longer core are practically negligible. The recovery and pressure

drop data from this run were used in the Welge type model to find the relative permeability parameters. Also the 0.2 cc/min. data from core # 3 was analyzed.

The ratio of parameters from these two experiments are shown as experimental point in Figures 7 to 10. This shows that although there is a functional relationship between the parameters and rate, the application of these functions to other cores is questionable.

5.2 IMBIBITION

The *true* relative permeabilities were calculated using the imbibition capillary pressure, and the recovery and pressure drop data from the 1 cc/min. imbibition run on core # 1. Figure 5.11 compares the experimental and history matched recovery and pressure drop data.

Obviously, the match is not as good as was obtained in case of drainage. The poor match is even more pronounced in the early time data. This is probably because of the spontaneous countercurrent imbibition. This occurs when the wetting phase comes in contact with the strongly water wet core sample. This effect is not yet modeled in the simulator. The *true* relative permeability is compared with the steady state curve in Figure 5.12. These curves show the same trend as those for the drainage case. The endpoint relative permeability is greater in case of displacement.

I tried to obtain the functional relationship between the relative permeability parameters and the dimensionless rate. But I could not find any trend in the data at the low rates.

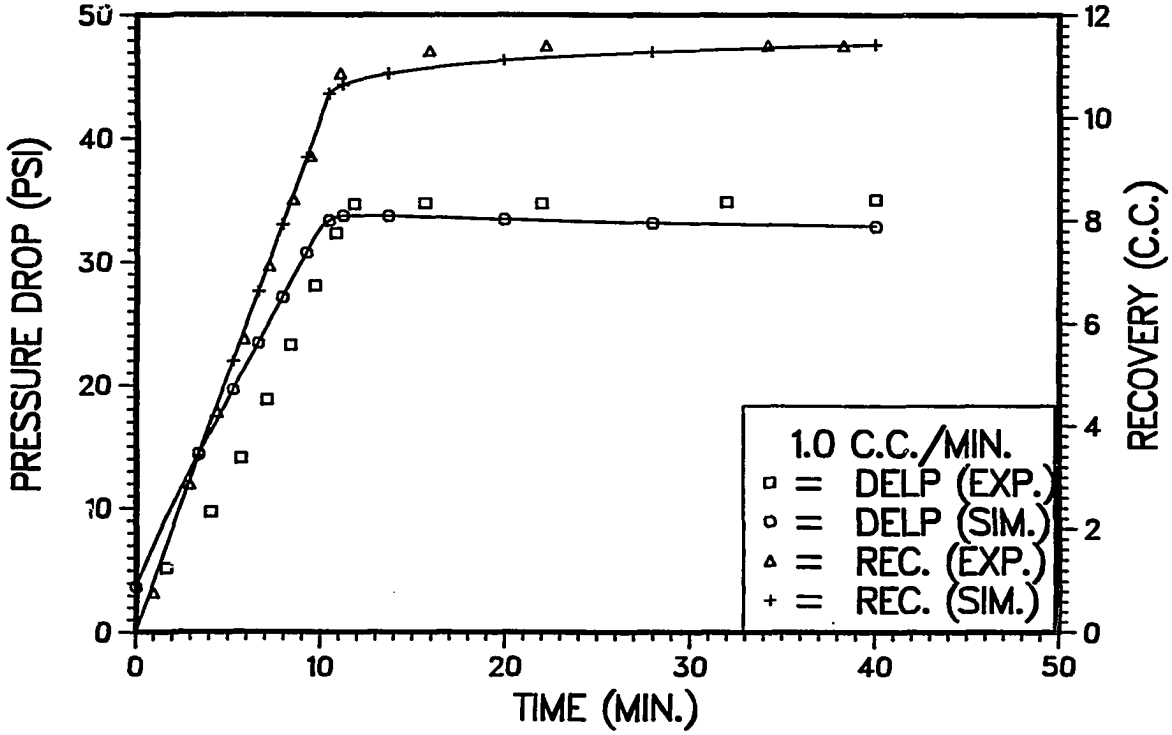

Fig. 5.11 Experimental and simulated recovery and pressure drop data for 1.0 cc/min. imbibition run on core # 1

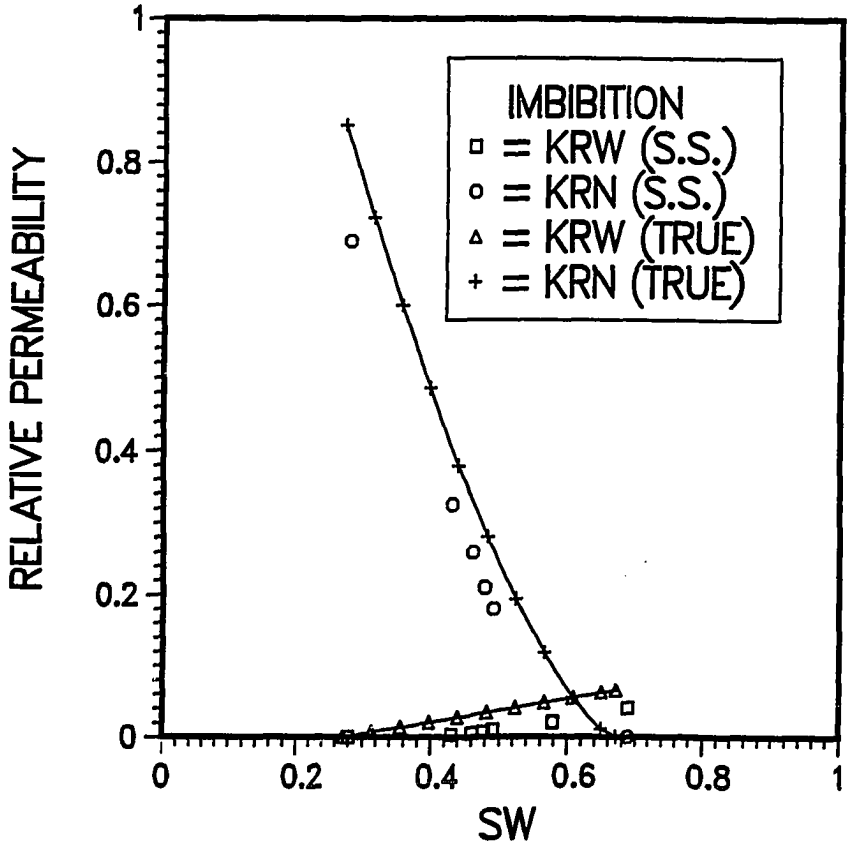

Fig. 5.12 Comparison of steady state and true imbibition relative permeability curves for core # 1.

6. CONCLUSIONS

In this study computer software is developed to calculate relative permeabilities from displacement data by history matching. Two models are developed to model the displacement process. One is a numerical simulator which included the capillary end effect and the other is a non–capillary Welge type model. The relative permeability curves are used in a parametric form. Also steady state and displacement experiments are conducted in different core samples using several rates. Using the experimental and simulated data, the effect of rate on the parameters describing the relative permeabilities is evaluated. From the results presented in this study the following is concluded:

1. In the case of drainage, the end point relative permeability and the saturation exponent for the non–wetting phase can be related to the dimensionless rate. Both parameters increased as the dimensionless rate is increased.

2. The saturation exponent in the wetting phase relative permeability function decreased as the dimensionless rate is increased.

3. The results of this study also showed that the end point relative permeability essentially do not change as the dimensionless rate is increased.

4. In the case of imbibition no meaningful rate dependent trend is observed for either the end point relative permeabilities or the saturation exponents.

5. In case of strongly water wet system, the inlet end effect, makes the imbibition displacement process more difficult to model than the drainage process.

6. The parametric representation of the relative permeability curves used in this study adequately describes the curves.

7. RECOMMENDATIONS

After analyzing the results obtained in this study, the following recommendations are made for future extension of this work.

1. It is important to study the counter current imbibition occurring in strongly water wet systems at the beginning of an imbibition displacement process. This will allow the inlet end effect to be included into a simulator needed to study the effect of rate on relative permeability parameters.

2. The software should be integrated with a computerized data acquisition system. This will eliminate manual digitization of the pressure drop data and entry of this data into computer, thus saving valuable time and reducing the chances of errors.

3. To refine the correlations presented in this study more data should be obtained using different viscosity fluids and core samples having different properties. This would give more accurate equations which can be applied to other rocks.

8. NOMENCLATURE

A	cross-sectional area
B	formation volume factor
c	geometric constant in Kozeny equation
D	accumulation matrix
f	fractional flow
f_w	fractional flow of water
k_r	relative permeability
k	permeability
L	length
p	pressure
$\vec{P}$	vector of pressures
P_c	capillary pressure
q	volumetric flow rate per unit time.
Q	flow rate
R	residual vector
RS	residual vector based on saturation
S	saturation
S_w	wetting phase saturation
S_n	non–wetting phase saturation
t	time
T	transmissibility matrix
V	volume
x	distance

Greek Symbols

θ	angle between horizontal and flow direction
λ	transmissibility
μ	viscosity
ρ	density
ϕ	porosity
τ	tortuosity

Subscripts

av	average
c	capillary
i	irreducible
n	non-wetting phase property
r	relative
w	wetting phase property
s_w	fixed saturation

9. BIBLIOGRAPHY

Amaefule, J.O. and Handy, L.L.: " The Effect of Interfacial Tension on Relative Oil-Water Permeabilities of Consolidated Porous Media", *SPE/DOE* 9783 presented at the SPE/DOE Second Joint Symposium, Tulsa, Oklahoma, (April, 1981)

Archer, J.S. and Wong, S.W.: "Use of Reservoir Simulator to Interpret Laboratory Water flood Data", *SPEJ*, (December 1973), 343–347

Ashford, F.E.: " Computed Relative Permeability; Drainage and Imbibition", *SPE* paper 2582 presented at 44th Annual Fall SPE Meeting, Denver, (Sept. 28 – Oct. 1, 1969.)

Aziz, K. and Settari, A.: Petroleum Reservoir Simulation, Elsevior Applied Science Publishers, London, (1979).

Braun, E.M. and Blackwell, R.J.: "A Steady–State Technique for Measuring Oil–Water Relative Permeability Curves at Reservoir Conditions", *SPE 10155*, presented at the 60th Annual Technical Conference and Exhibition of SPE San Antonio, TX (Oct. 5–7, 1981)

Brownscombe, E.R., Slobod, R.L., and Caudle, B.H.: "Relative Permeability", *Parts I and II, Oil and Gas J.*, (Feb. 9 & 16, 1950) 68– 69 and 98–102.

Buckley, S.E. and Leverett, M.C. "Mechanism of Fluid Flow in Sands", *Trans. AIME*, (1942), **146**, 107–116

Burdine, N.T., Gournay, L.S., and Reichertz, P.P.: "Pore Size Distribution of Reservoir Rocks", *Trans. AIME*, (1950), **189**, 195–204.

Burdine, N.T.: "Relative Permeability Calculations from Pore Size Distribution Data", *Trans. AIME* (1953), **198**, 71–77.

Caudle, B.H., Slobod, R.L., and Brownscombe, E.R.: "Further Developments in the Laboratory Determination Of Relative Permeability", *Trans. AIME* (1951), **192**, 145–150

Chatenever, A. and Calhoun, J.C. Jr.: "Visual Examination of Fluid Behavior in Porous Media–Part 1", *Trans. AIME*, (1952), **195**, 149–156

Chouke, R.L.,Van Meurs, P., and Vander Poel, C.: "The Instability of Slow, Immiscible, Viscous Liquid–Liquid Displacements in Permeable Media", *Trans. AIME*, (1959) **216**, 188–194

Civan, F. and Donaldson, E.C.: "Relative Permeability from Unsteady State Displacements: An Analytical Interpretation", *SPE 16200* presented at SPE Production Operation Symposium, Oklahoma City OK (March 8–10, 1987)

Corey, A.T.: "The Interrelation Between Gas and Oil Relative Permeabilities", *Prod. Monthly*, (Nov. 1954), 38–41.

Corey, A.T.: Mechanics of Heterogenous Fluids in Porous Media, Water Resources Publ., Fort Collins, (1977).

Dullien, F.A.L.: Porous Media: Fluid Transport and Pore Structure, Academic Press, New York (1979).

Fatt, I. and Dykstra, H.: "Relative Permeability Studies",*Trns. AIME*, (1951), **207**, 144–159.

Fletcher, R.: Practical Methods of Optimization, John Wiley (1981).

Gabrieal, G.A. and Inamdar, G.R.: "An Experimental Investigation of Fines Migration in Porous Media", *SPE 12168*, Presented at the 58th Annual Technical Conference of SPE, San Francisco, CA. (October 5–8, 1983)

Gates, J.I. and Lietz, W.T.: "Relative permeabilities of California Cores by Capillary Pressure Method", *Drilling and Prod. Practice*, (1950), 285–301.

Geffen, T.M., Owens, W.W., Parrish, D.R., and Morse, R.A.: "Experimental Investigation of Factors Affecting Laboratory Relative Permeability Measurements", *Trans. AIME*, (1951), **192**, 99–110

Hadley, G.F. and Handy, L.L.: "A Theoretical and Experimental Study of The Steady State Capillary End Effect", *SPE Paper 707-G* presented at the 31st Annual Fall Meeting of the Petroleum Branch of the AIME, (October 14–17, 1956)

Handy, L.L. and Data, P.: "Fluid Distributions During Immiscible Displacements in Porous Media", *SPEJ* (September 1966) 261–266

Hassler, G.L., Rice, R.R. and Leeman, E.H.: "Investigation on the Recovery of Oil from Sandstones by Gas Drive", *Trans. AIME* (1936), **118**, 116

Hassler, G.L.: "Methods and Apparatus for Permeability Measurements", *U.S. Pat. No. 2,345,935*, (1944)

Heaviside, J. and Black, C.J.J.: "Fundamentals of relative permeability: Experimental and Theoretical Considerations.",*SPE 12173* presented at the 58th Annual Technical Conference of SPE–AIME, San Francisco (October 5–8, 1983).

Hvolboll, V.T.: "Method for Accurately Measuring Produced Oil Volumes During Laboratory Waterflood Test at Reservoir Conditions", *SPEJ*, (Aug. 1978), 239–241

Johnson, E.F., Bossler, D.P., and Neumann, V.O.: "Calculation of Relative Permeability From Displacement Experiments", *Trans. AIME* (1959), **216**, 370–372

Jones, S.C. and Roszelle, W.O.: "Graphical Techniques for Determining Relative Permeability From Displacement Experiments", *JPT*, (May 1978), 807–817.

Kuester, J.L. and Mize, J.H.: Optimization Techniques with Fortran, McGraw Hill, New York City (1973) 218–242.

Leverett, M.C.: "Flow of Oil–Water Mixtures through Unconsolidated Sands", *Trans. AIME* (1939), **132**, 149–171

Leverett, M.C.: "Capillary Behavior in Porous Media", *Trans. AIME* (1941), **142**, 152–169

Loomis, A.G. and Crowell, D.C.: "Relative Permeability Studies: Gas–Oil and Water–Oil Systems", *Bull. 599 U.S.B.M.*, (1962).

Morrow, N.R. and Chatiudompunth, S.: " Application of Hydraulic Radii Concept to Multiphase Flow", PRRC report 80–48, New Mexico Pet. Rec. Res. Center, Socorro, New Mexico (1980).

Morse, R.A., Terwilliger, P.L. and Yuster, S.T.: "Relative Permeability Measurements on Small Core Samples", *Oil & Gas J.*, (Aug., 1947), 109.

Narr, J. and Henderson, J.H.: "An Imbibition Model – Its Application to Flow Behavior and The Prediction of Oil Recovery", *SPEJ* (June 1961), 61–70.

Narr, J., Wygal, R.J. and Henderson, J.H.: "Imbibition Relative Permeability in Unconsolidated Porous Media", *SPEJ* (March 1962) 13–17.

Odeh, A.S. and Dotson, B.J.: "A Method for Reducing the Rate Effect on Oil and Water Relative Permeabilities Calculated from Dynamic Displacement Data", SPE 14417 presented at the 60th Annual Technical Conference of SPE, Las Vegas, NV (September 22-25, 1985)

Osoba, J.S., Richardson, J.G., Kerver, J.K., Hafford, J.A., and Blair, P.M.: "Laboratory Measurements Of Relative Permeability", *Trans. AIME* (1951), 192 47–56

Owen, W.W., Parish, D.R. and Lamoreaux, W.E.: "An Evaluation of a Gas Drive Method for Determining Relative Permeability Relationship", *Trans. AIME*, (1956), **207**, 275–280.

Peters, E.J. and Flock, D.L.: "The Onset of Instability During Two–Phase Immiscible Displacement in Porous Media", *SPEJ*, (April 1981), 249–258

Purcell, W.R.: "Capillary Pressures–Their Measurement Using Mercury And The Calculation of Permeability Therefrom", *Trans. AIME*, (1949), **186**, 39–48

Rapoport, L.A. and Leas, W.J.: "Relative Permeability to Liquid in Liquid–Gas System", *Trans. AIME* (9151), **192**, 83–98

Rapoport, L.A. and Leas, W.J.: "Properties of Linear Waterfloods", *Trans. AIME* (1953), **198**, 139–148

Reklaitis, G.V., Ravindram, A. and Ragsdell, K.M.: Engineering Optimization Methods and Applications, John Wiley and Sons, New York City (1983).

Richardson, J.G.: "The Calculation of Water Flood Recovery from Steady state Relative Permeability Data", *Trans. AIME*, (1957), **210**, 373–375.

Saraf, D.N., Batycky, J., Jackson, C.H. and Fisher, D.B.: "An Experimental Investigation of Three–Phase Flow of Water–Oil–Gas Mixtures Through Water–Wet Sandstones", *SPE 10761*, presented at the 1982 California Regional Meeting of SPE, San Francisco, CA (March 24–26, 1982).

Saraf, D.N. and McCaffery, F.G.: "Two and Three Phase Relative Permeabilities: A Review", Petroleum Recovery Institute Report No. 81–8, (Sept 1981).

Scheidegger, A.E. : The Physics of Flow Through Porous Media, Univ. of Toronto Press (1974).

Schilthuis, R. J. "Connate Water in Oil and Gas Sands", *Trans. AIME*, (1938), **127**, 199–214.

Settari, A.: Numerical Simulation of Three phase Coning in Petroleum Reservoirs, *Ph. D. Thesis*, The University of Calgary (9173).

Settari, A. and Aziz, K.: "A Computer Model for Two Phase Conning Simulation", *SPEJ*, (June 1974) 221–236.

Settari, A. and Aziz, K.: "Treatment of Nonlinear Terms in the Solution of Partial Differential Equations for Multiphase Flow", *Int. J. Multiphase Flow*, (1978), **1**, 817–844.

Sigmund, P.M. and McCaffery, F.G.: "An Improved Unsteady–State Procedure for Determining the Relative Permeability Characteristics of Heterogenous Porous Media", *SPEJ*, (February 1979), 15-28

Tao, T.M. and Watson, A.T.: "Accuracy of JBN Estimates of Relative Permeability: Part 1 – Error Analysis", *SPEJ*, (April 1984), 209–214

Tao, T.M. and Watson, A.T.: "Accuracy of JBN Estimates of Relative Permeability: Part 2 – Algorithms", *SPEJ*, (April 1984), 215–223

Terwilliger, P.L., Wilsy, L.E., Hall, H.N. Bridges, P.M. and Morse, R.A.: "An Experimental and Theoretical Investigation of Gravity Drainage Performance", *Trans. AIME*, (1951), **192**, 285–296.

Torabzadeh, S.J. and Handy, L.L.: "The Effect of Temperature and Interfacial Tension on Water–Oil Relative Permeabilities of Consolidated Sand", *SPE 12689*, presented at the SPE 1984 California Regional Meeting, Long Beach, CA, (April 11–13, 1984).

Watson, A.T. and Kerig, P.D., Richmond, P.C., and Tao, T.M.: "An Improved Method for Estimating Relative Permeability From Displacement Experiments", *SPE 15064*, presented at the SPE 1986 California Regional Meeting, Oakland, CA, (April 2–4, 1986)

Welge, H.J.: "A Simplified Method For Computing Oil Recovery By Gas or Water Drive", *Trans. AIME*, (1952), **195**, 91–98

Willhite G.P.: Waterflooding, *SPE* (1986).

Wyckoff, R.D. and Botset, H.G. "Flow Through Unconsolidated Sands", *Physics* (Sept.1936), 7

Wyllie, M.R.J. and Gardner, G.H.F.: " The Generalized Kozeny–Carman Equation," Parts I and II, *World Oil* (March & April 1958) 121–128 & 210–227.

APPENDIX

(Experimental Data)

Table A.1: Data from capillary pressure experiments

Length = 2.59 cm Diameter = 2.54 cm V_p = 3.2 cc

Speed RPM	ΔV cc	$\overline{S_w}$
Drainage		
500	0.0	0.625
1000	0.40	0.500
1290	0.60	0.438
1400	0.70	0.406
1600	0.80	0.375
1800	0.90	0.344
2200	1.10	0.281
2400	1.15	0.266
2800	1.25	0.234
3400	1.35	0.203
Imbibition		
3000	2.05	0.146
1000	1.81	0.246
750	1.77	0.263
500	1.27	0.471
0	1.25	0.479

Table A.2: Core # 1 1.0 cc/min drainage displacement data

Time min	Pressure drop psi	Recovery cc
0.2	33.4	0.2
0.3	33.7	0.3
0.6	33.8	0.6
0.9	33.7	0.9
1.2	33.6	1.2
1.6	33.2	1.6
3.2	31.0	2.8
4.6	28.6	4.7
6.6	25.5	6.1
8.0	23.5	6.3
9.4	22.0	6.6
11.9	19.9	6.8
14.1	18.4	7.1
17.4	16.8	7.3
21.0	15.5	7.4
24.5	14.4	7.6
27.4	13.7	7.9
30.2	13.2	7.9
36.2	12.3	8.2
47.8	11.1	8.5
52.5	10.7	8.6
64.2	10.0	8.8

84.1	9.1	8.9
108.0	8.4	9.2
159.4	7.6	9.5
184.1	7.4	9.7
225.4	7.1	9.8
256.4	7.0	10.0

Table A.3: Core # 1 0.5 cc/min drainage displacement data

Time min	Pressure drop psi	Recovery cc
0.2	12.1	0.1
0.3	17.7	0.1
1.3	18.4	0.6
2.2	18.2	1.1
4.1	17.7	2.1
6.1	16.7	2.2
8.1	15.8	2.2
10.1	14.8	5.7
12.2	13.6	6.2
14.1	12.8	6.3
18.2	11.4	6.3
20.2	10.8	6.3
22.3	10.3	6.6
24.2	9.8	7.0
26.2	9.4	7.1
28.2	9.1	7.2
30.3	8.7	7.3
32.3	8.5	7.4
34.3	8.2	7.4
36.3	8.0	7.5
38.3	7.8	7.6
40.4	7.6	7.6

42.4	7.5	7.6
44.3	7.3	7.6
46.3	7.2	7.8
48.4	7.1	7.8
50.4	7.0	7.8
50.4	6.9	7.8
54.4	6.6	7.9
58.4	6.4	8.0
62.3	6.3	8.1
66.5	6.1	8.1
70.4	5.9	8.1
74.5	5.8	8.2
78.5	5.8	8.3
82.4	5.6	8.3
85.1	5.6	8.3
89.1	5.5	8.4
94.5	5.3	8.4
98.5	5.3	8.5
102.5	5.2	8.4

Table A.4: Core # 2 2.0 cc/min drainage displacement data

Time min	Pressure drop psi	Recovery cc
1.0	20.9	0.6
1.7	20.2	2.1
2.4	19.1	3.6
3.1	17.8	4.7
4.3	15.7	6.6
5.7	14.1	7.0
7.8	12.7	7.4
9.7	11.7	7.6
11.7	11.0	7.8
13.8	10.4	8.0
15.7	10.0	8.1
17.6	9.6	8.3
19.7	9.4	8.4
21.7	9.1	8.5
23.7	8.7	8.6
25.4	8.6	8.7
27.7	8.4	8.9
29.7	8.3	9.0
31.7	8.2	9.2
33.8	8.0	9.2
37.6	7.8	9.1
61.4	7.1	9.8

85.3	6.6	10.2
108.8	6.4	10.4
133.3	6.2	10.6
160.1	6.0	10.8
181.6	5.9	10.9
205.2	5.9	11.1
225.3	5.8	11.1
253.1	5.8	11.0
277.0	5.7	11.2
301.4	5.6	11.4

Table A.5: Core # 3 0.2 cc/min drainage displacement data

Time min	Pressure drop psi	Recovery cc
1.0	2.4	0.1
3.0	2.3	0.4
4.3	2.3	0.7
9.0	2.0	1.5
13.0	1.8	2.3
16.9	1.7	2.8
20.9	1.6	3.0
24.9	1.5	2.9
28.9	1.5	3.0
32.9	1.4	3.1
36.8	1.4	3.3
41.0	1.4	3.3
45.0	1.4	3.3
48.8	1.4	3.4
52.9	1.3	3.4
57.0	1.3	3.4
61.0	1.3	3.4
65.0	1.3	3.5
69.0	1.3	3.5
72.8	1.3	3.5
76.9	1.3	3.6
80.9	1.2	3.6

84.9	1.2	3.6
88.9	1.2	3.6
93.0	1.2	3.7
96.9	1.2	3.7

Table A.6: Core # 1 1.0 cc/min imbibition displacement data

Time min	Pressure drop psi	Recovery cc
1.0	6.7	0.8
1.7	8.0	1.6
2.4	9.7	2.3
3.0	10.9	2.9
3.6	12.7	3.5
4.0	14.1	4.1
4.4	15.6	4.3
4.9	17.2	4.7
5.4	18.9	5.3
5.9	20.2	5.7
6.2	21.8	6.0
6.7	23.3	6.6
7.2	24.9	7.1
7.5	26.4	7.4
8.0	28.0	7.8
8.5	29.6	8.4
8.8	30.8	8.7
9.2	32.3	9.0
9.4	33.6	9.2
9.5	34.4	9.3
10.1	34.7	10.1
11.1	34.7	10.8

12.0	34.7	11.2
14.0	34.7	11.3
15.9	34.8	11.3
18.2	34.7	11.4
20.3	34.7	11.4
22.2	34.7	11.4
26.2	34.8	11.4
30.3	34.8	11.4
34.2	34.9	11.4
38.3	35.0	11.4

Table A.7: Core # 1 steady–state relative permeability data

Q_w cc/min	Q_n cc/min	ΔS_w	ΔP psi
Drainage			
2.0	–	0.373	87
1.8	0.2	0.037	114
1.2	0.8	0.047	138
0.4	1.6	0.050	84
0.3	1.7	0.010	72
0.2	1.8	0.017	58
0.15	1.85	0.01	51
0.03	1.94	0.02	33
0.03	1.97	0.04	25
–	2.0	0.134	10
Imbibition			
0.2	1.8	0.013	38
0.4	1.6	0.033	72
0.8	1.2	0.037	123
1.0	1.0	0.013	138
1.1	0.9	0.007	142
2.0	–	.094	111